IMPROVED SENSITIVITY OF SURFACE PLASMON RESONANCE
SENSOR USING OPTICAL RELAY SETUP

WARAMANEE NETPHRUEKSARAT

A Thesis Submitted in Partial Fulfillment of the Requirements for the Degree of
Master of Engineering in Electrical Engineering
Suranaree University of Technology
Academic Year 2022

การพัฒนาความไวของเซนเซอร์แบบคลื่นผิวพลาสมอนโดยใช้การติดตั้งระบบแบบถ่ายทอดทางแสง

นางสาววรามณี เนตรพฤษรัตน์

วิทยานิพนธ์นี้เป็นส่วนหนึ่งของการศึกษาตามหลักสูตรปริญญาวิศวกรรมศาสตรมหาบัณฑิต
สาขาวิชาวิศวกรรมไฟฟ้า
มหาวิทยาลัยเทคโนโลยีสุรนารี
ปีการศึกษา 2565

IMPROVED SENSITIVITY OF SURFACE PLASMON RESONANCE SENSOR USING OPTICAL RELAY SETUP

Suranaree University of Technology has approved this thesis submitted in partial fulfillment of the requirements for a Master's Degree.

Thesis Examining Committee

_____

(Asst. Prof. Dr. Boonsong Sutapun)

Chairperson

_____

(Prof. Dr. Joewono Widjaja)

Member (Thesis Advisor)

_____

(Dr. Siriwat Soontaranon)

Member

_____
(Assoc. Prof. Dr. Chatchai Jothityangkoon)
Vice Rector for Academic Affairs and
Quality Assurance

_____
(Assoc. Prof. Dr. Pornsiri Jongkol)
Dean of Institute of Engineering

วรามณี เนตรพฤษรัตน์ : การพัฒนาความไวของเซนเซอร์แบบคลื่นผิวพลาสมอนโดยใช้การ
ติดตั้งระบบแบบถ่ายทอดทางแสง (IMPROVED SENSITIVITY OF SURFACE PLASMON
RESONANCE SENSOR USING OPTICAL RELAY SETUP)
อาจารย์ที่ปรึกษา : ศาสตราจารย์ ดร. โจโวโน วิดจายา, 69 หน้า.

คำสำคัญ : เซนเซอร์แบบคลื่นผิวพลาสมอนเรโซแนนซ์/การติดตั้งแบบ 4-F/การวัดค่าดัชนีหักเหของ
แสง/ลำแสงแบบกระจาย/เซนเซอร์ทางชีวเคมี

วิทยานิพนธ์นี้ศึกษาการพัฒนาความไวของเซนเซอร์แบบคลื่นผิวพลาสมอนโดยใช้การติดตั้ง
ระบบแบบถ่ายทอดทางแสง งานวิจัยนี้ได้ใช้การศึกษาเชิงมุมโดยการใช้ลำแสงขนาดเล็กตัดกันภายใน
ปริซึมด้วยการติดตั้งระบบแบบ 4f ให้การตอบสนองเชิงเส้นของการวัดดัชนีการหักเหของแสง ในการ
บันทึกผลการทดลองใช้ CMOS เซนเซอร์ นอกจากนี้ยังใช้การปรับความเข้มข้นของกลีเซอรอล
ระหว่าง 0 ถึง 10% w/w ในการตรวจสอบยืนยันความถูกต้องในการทดลอง

สาขาวิชา วิศวกรรมอิเล็กทรอนิกส์   ลายมือชื่อนักศึกษา Waramanee Netphraebsarat
ปีการศึกษา 2565   ลายมือชื่ออาจารย์ที่ปรึกษา

WARAMANEE NETPHRUEKSARAT : IMPROVED SENSITIVITY OF SURFACE
PLASMON RESONANCE SENSOR USING OPTICAL RELAY SETUP. THESIS ADVISOR
: PROF. JOEWONO WIDJAJA, Ph.D., 69 PP.

Keyword : SURFACE PLASMON RESONANCE SENSOR/ 4-F OPTICAL SETUP/ REFRACTIVE
INDEX MEASUREMENT/ DIVERGENT BEAM BIOCHEMICAL SENSOR

This thesis proposes to increase the sensitivity of an angular interrogation-based surface plasmon resonance sensor by employing divergent beam illumination. A small divergent beam illumination produced within the prism with a 4f optical setup which is provided a linear response of refractive index measurements. Experiments show that the proposed method works by changing the amount of glycerol between 0 and 10% w/w.
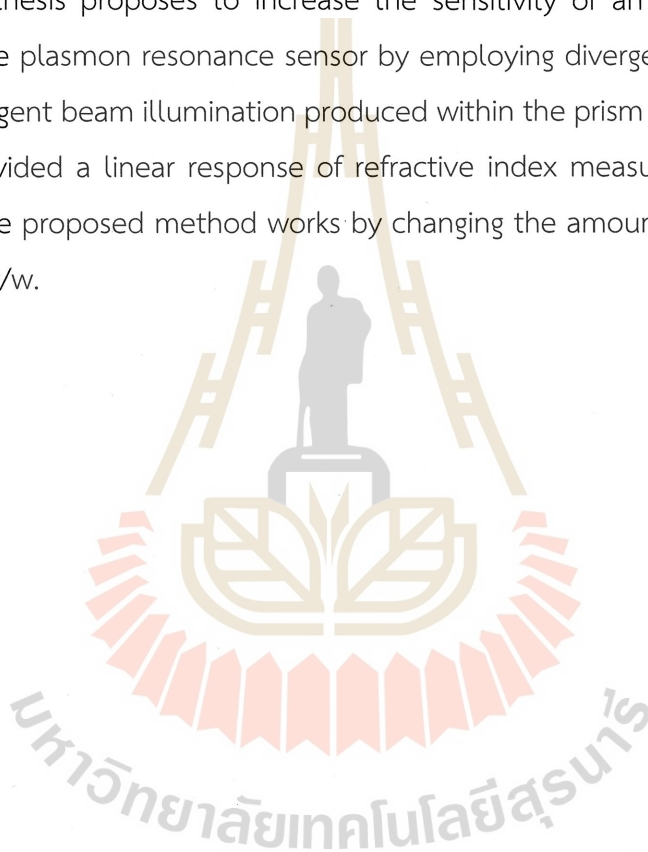
School of Electronic Engineering

Academic Year 2022

Student's Signature _Waramanee Netphrueksarat_

Advisor's Signature _Joewono_

ACKNOWLEDGEMENT

TABLE OF CONTENTS

Page

TABLE OF CONTENTS (Continued)

LIST OF TABLES

LIST OF TABLES (Continued)

LIST OF FIGURES

LIST OF FIGURES (Continued)

CHAPTER I

INTRODUCTION

1.1 SURFACE PLASMON RESONANCE SENSOR

Surface plasmon resonance (SPR) is an optical phenomenon that happens when parallel (p) polarized laser light is incident at an angle greater than the critical angle of a dielectric medium and a metal layer (Schasfoort, 2017). To generate a resonance state of surface plasmons at the media interface, the incident photon must have the wave vector and momentum that match with the plasmon. This resonance condition can be met by altering the incident angle of the photon. At a specific angle called the resonance angle, a sample put on top of the metal layer absorbs the incident photon's energy due to the plasmon resonance. Therefore, a dark band occurs on a specific portion of a pattern of reflected light. Due to wave vectors rely on refractive indices, it is possible to evaluate the refractive index of a dielectric material by detecting the dark band with light sensors.

There have been reports of SPR sensor applications in several domains, including medicine (Fathi et al., 2019) and biochemistry (Kabashin et al., 2009). In addition, it is real-time detection of the changes in refractive index of the sample (Bak et al., 2018; Wang et al., 2014). SPR sensors are label-free (Kodoyianni, 2011) and noninvasive (Firdous et al., 2018). SPR sensors can detect small changes in the refractive index of low-volume samples with shorter preparation time compared to conventional chemical methods (Liu et al., 2018). SPR sensor is useful for healthcare monitoring (Puiu et al., 2016), including ovarian cancer diagnosis (Szymanska et al., 2021) and assessment of morphine specificity in urine samples (Ke et al., 2020). Recent reports indicate that the detection of ligan, antigen-antibody, and CO_2 reactions for indoor and outdoor applications have been successful. (Mudgal, 2020; Pérez-Ocón et al., 2021).

The Kretschmann configuration, which comprise of a prism, a thin metal layer as a sensor chip, and a dielectric sample to be studied, is a suitable way for developing

SPR sensors. The beam which is incident reaches the sensor chip's interface from within the prism in the Kretschmann design. When the conditions for plasmon resonance are achieved, the energy of the photon from the incident beam is absorbed, causing a decrease in the intensity of the reflected light at the resonance angle. Since the resonance angle relies on the refractive index of samples, altering the incidence angle of photons allows for the detection of various types of samples. An angular interrogation is a type of SPR sensor since it evaluates samples in accordance with the angular sensing response. It can be achieved by rotating either a light laser source or the prism, which produces an increase in the sensor system's complexity and size (Lan et al., 2015; Ruemmele et al., 2008). To solve this problem, a LED (Chinowsky et al., 2003), a cylindrical lens (Chan et al., 2014), a quantum cascade laser (Herminjard et al., 2009) and a laser diode (Isaacs et al., 2015) have been applied to create the SPR sensor. This is because the diverging beam is composed of a collection of light rays traveling at different angles. However, it provides a Gaussian distribution beam profile, which may not generate a well-defined SPR reflectivity drop.

A Powell lens, also called a laser line generator, produces a uniform distribution of light energy from laser beams (Powell, 1989). Several approaches have been presented for implementing SPR sensors using Powell lens SPR sensors. An implementation of a multichannel SPR has been presented by translating a small divergent beam created at the interface of the prism and the metal layer where an array of samples is positioned. A translation stage is utilized to translate the beam by moving the Powell lens attached to a laser source (Chen et al., 2015; Hu et al., 2016). Consequently, this method has the same mechanical scanning issues as the conventional ones. The second concept utilizes the Fourier transform feature of a thin lens to refract parallel beams from different positions in a front focal plane with respect to a back focal plane. When a spatially shifted parallel beam illuminates the lens, the output beam will be refracted at a different angle of refraction. The revolving slit is used to scan the input divergent beam and the metal layer is placed at the BFL of the lens, angular interrogation can be implemented (Patskovsky et al., 2013). However, the mechanical rotation of the motor generates noise and vibration which reduces measurement accuracy. A method for improving the SPR system utilizing a

Powell lens without mechanical movement was reported as a solution to this issue (Widjaja et al., 2021). This is easily accomplished by illuminating the three-layer Kretschmann setup directly with a divergent beam produced by a Powell lens. In addition to being free of noise and vibration, a broad evanescent wave production provides an advantage over earlier methods in that numerous samples' refractive indices may be evaluated in real time using a simple setup. However, internal and external refraction of the beam enlarges the output beam size incident on the light detector. This demands a costly and large-sized image sensor.

1.2   SIGNIFICANCE OF THE STUDY

In this work, we propose a novel methodology for enhancing SPR sensitivity by applying a small divergent light beam detected by a small image sensor. Conversely to the prior method (Widjaja et al., 2021), the Powell lens produces the beam output which is imaged within the prism utilizing a 4f optical setup, resulting in a small incident beam on the gold sensor chip. In addition to keeping a wide divergence angle of the generated beam within the prism, the 4f arrangement provides a linear response to refractive index measurements and enhances the SPR sensitivity. By measuring the refractive indices of glycerol with concentrations ranging from 0 to 10% (w/w), the experimental viability of the suggested method for building a multi-channel SPR sensor is demonstrated.

1.3   RESEARCH OBJECTIVES

1.3.1   To design and implement the SPR sensor with the readout beam that diverges inside the prism.

1.3.2   To evaluate the sensitivity of the proposed SPR system.

1.4   SCOPE OF THESIS

1.4.1   To measure refractive index of glycerol from 0 - 10% w/w concentration

1.4.2   To verify experimentally the feasibility of the proposed SPR system.

1.4.3   To evaluate the sensitivity of the proposed SPR system.

1.5   ORGANIZATION OF THE THESIS

The thesis contains five chapters. The first chapter covers the research motivation, significance, aims, and scope of the study. The theories of surface plasmon resonance and refractive index mixture rules are covered in Chapter 2. The proposed SPR sensor is discussed in Chapter 3. Chapter 4 discusses the experimental measurements of glycerol refractive index and the sensitivity performance. The final chapter summarizes the present research work.
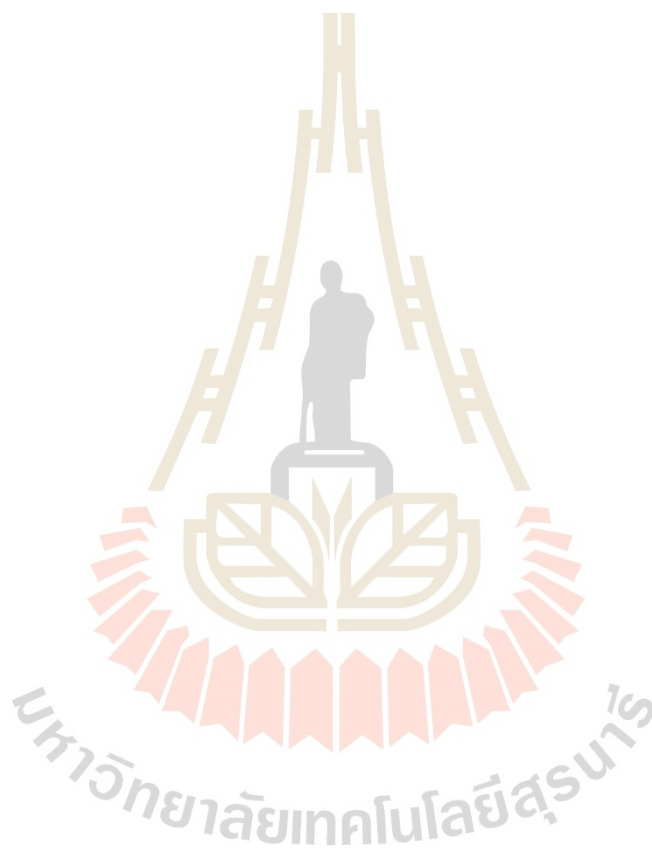
CHAPTER II

THEORY

2.1   GENERAL THEORY OF SURFACE PLASMON

The surface plasmons are electron oscillations with a well defined frequency and wave vector that exist at the interface of a metal-dielectric interface. The plasmons will resonate when an external electric field is applied to the interface with the wave vector matching the parallel wavevector of the plasmon (Schasfoort, 2017). This condition is only satisfied by p-polarized light, in which the electric field vector is parallel to the plane of incidence. On the other hand, s-polarized light cannot support the generation of the surface plasmon resonance because the wave vector condition is violated. In addition, the surface plasmon resonance using s-polarized light requires magnetic materials with different polarities that cannot be found.
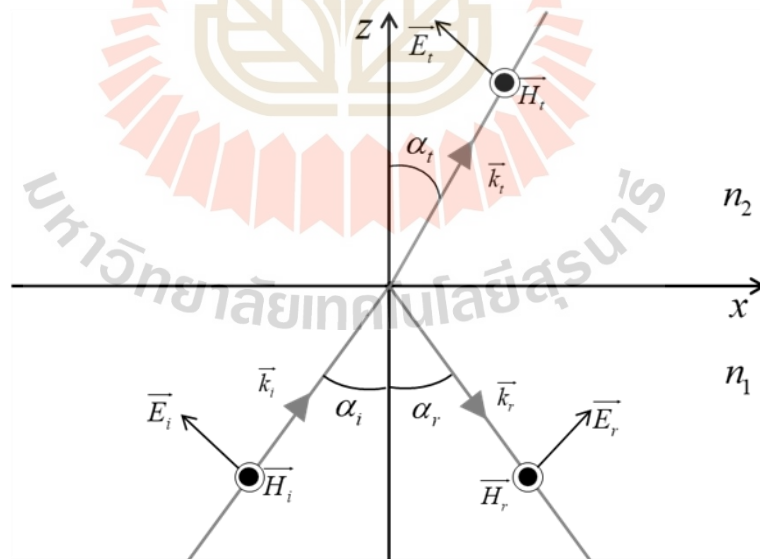
Figure 2.1 P-polarized wave incident to the interface between two mediums, n_1 and n_2.

Figure 2.1 shows the p-polarized wave incident to the interface between two media 1 and 2 having the refractive indices of n_1 and n_2, respectively. The angles α_i, α_r and α_t represent the incident, refracted, and transmitted angles of the three waves, respectively. k_i, k_r and k_t are the wave vector of the incident, refracted, and transmitted wave that can be expressed by

$$k_i = k_i \sin\alpha_i \vec{a_x} + k_i \cos\alpha_i \vec{a_z}, \tag{2.1}$$

$$k_r = k_r \sin\alpha_r \vec{a_x} - k_r \cos\alpha_r \vec{a_z} \tag{2.2}$$

and

$$k_t = k_t \sin\alpha_t \vec{a_x} + k_t \cos\alpha_t \vec{a_z} \tag{2.3}$$

Here, $\vec{a_x}$, $\vec{a_y}$ and $\vec{a_z}$ are the unit vectors. The electric fields of the incident and transmitted waves that are parallel to the incident plane or x-z plane are given by

$$\vec{E_i}(x,z) = E_{io}\left(-\vec{a_x}\cos\alpha_i + \vec{a_z}\sin\alpha_i\right)\exp\left[-jxk_i\sin\alpha_i\right]\exp\left[-jzk_i\cos\alpha_i\right] \tag{2.4}$$

and

$$\vec{E_t}(x,z) = E_{to}\left(-\vec{a_x}\cos\alpha_t + \vec{a_z}\sin\alpha_t\right)\exp\left[-jxk_t\sin\alpha_t\right]\exp\left[-jzk_t\cos\alpha_t\right] \tag{2.5}$$

with E_{io} and E_{to} are the amplitude of incident and transmitted fields, respectively. The corresponding magnitude of the incident and transmitted magnetic fields which are perpendicular to the electric fields can be written as

$$\vec{H_i}(x,z) = \frac{\vec{a_y}E_{io}}{\eta_1}\exp\left[-jxk_i\sin\alpha_i\right]\exp\left[-jzk_i\cos\alpha_i\right] \tag{2.6}$$

And

$$\vec{H_t}(x,z) = \frac{\vec{a_y}E_{to}}{\eta_2}\exp\left[-jxk_t\sin\alpha_t\right]\exp\left[-jzk_t\cos\alpha_t\right] \tag{2.7}$$

where η_1 and η_2 are the instinsic impedances of the mediua 1 and 2, respectively.

2.2   EVANESCENT WAVE

When the incidence angle of the p-polarized light is larger than the critical angle, the external electric field, also known as an evanescent wave, will occur (Tang, 2019). According to Snell's law of refraction, the critical angle α_c can be expressed mathematically

$$\alpha_c = \sin^{-1}\left(\frac{n_2}{n_1}\right) \tag{2.8}$$

with $n_1 > n_2$. At this specific incidence angle, the incident light is reflected by the incident medium. For the refracted wave, it is converted into a so-called evanescent wave that propagates along the surface boundary with exponentially decreasing amplitude as the propagation depth increases. When the incidence angle is larger than the critical angle,

$$\sin \alpha_t = \frac{n_1}{n_2} \sin \alpha_i . \tag{2.9}$$

By expressing

$$\cos \alpha_t = \pm j \sqrt{\left(\frac{n_1}{n_2}\sin\alpha_i\right)^2 - 1}, \tag{2.10}$$

the transmitted electric field of Eq. (2.5) or the evanescent wave can be expressed as

$$\vec{E}_t(x,z) = E_{to}\left(-\vec{a}_x\cos\alpha_t + \vec{a}_z\sin\alpha_t\right)\exp\left[-jxk_t\frac{n_1}{n_2}\sin\alpha_i\right]$$
$$\times \exp\left[\pm zk_t\sqrt{\left(\frac{n_1}{n_2}\sin\alpha_i\right)^2 - 1}\right] \tag{2.11}$$

and can be simplified to

$$\vec{E_t}(x,z) = E_{to}\left(-\vec{a_x}\cos\alpha_t + \vec{a_z}\sin\alpha_t\right)\exp\left[-jk_xx\right]\exp\left[-Az\right] \qquad (2.12)$$

The function *A* is

$$A = k_t\sqrt{\left(\frac{n_1}{n_2}\sin\alpha_i\right)^2 - 1} \qquad (2.13)$$

and

$$k_x = k_i\frac{n_1}{n_2}\sin\alpha_i, \qquad (2.14)$$

which is the evanescent wave's wave vector.

2.3 SURFACE PLASMON

To achieve the SPR, the p-polarized light is required as mentioned in section 2.1.

Figure 2.2 Propagation of the P-polarized wave along the interface
between the metal and the dielectric layers.

Figure 2.2 shows the diagram of the p-polarized wave travels at the interface between the gold and the dielectric layers at z=0. The evanescent waves at each medium are given by

$$\overrightarrow{E_{t1}}(x,z) = E_{to}\left(-\overrightarrow{a_x}\cos\alpha_{t1} + \overrightarrow{a_z}\sin\alpha_{t1}\right)\exp\left[-jk_x x\right]\exp\left[A_1 z\right] \text{for } z<0 \quad (2.15)$$

and

$$\overrightarrow{E_{t2}}(x,z) = E_{to}\left(-\overrightarrow{a_x}\cos\alpha_{t2} + \overrightarrow{a_z}\sin\alpha_{t2}\right)\exp\left[-jk_x x\right]\exp\left[-A_2 z\right] \text{for } z>0 \quad (2.16)$$

According to the wave equation, the evanescent wave propagation through the gold layer follows

$$\frac{\partial^2 \overrightarrow{E_{t1}}(x,z)}{\partial^2 x} + \frac{\partial^2 \overrightarrow{E_{t1}}(x,z)}{\partial^2 y} + \frac{\partial^2 \overrightarrow{E_{t1}}(x,z)}{\partial^2 z} = \mu_1\varepsilon_1\frac{\partial^2 \overrightarrow{E_{t1}}(x,z)}{\partial^2 t}. \quad (2.17)$$

Substitution of Eq. (2.15) into Eq. (2.17) gives

$$-k_x^{\ 2}\overrightarrow{E_{t1}}(x,z) + A_1^{\ 2}\overrightarrow{E_{t1}}(x,z) = -\omega^2\mu_1\varepsilon_1\overrightarrow{E_{t1}}(x,z). \quad (2.18)$$

Division of both sides in Eq. (2.18) by $\overrightarrow{E_{t1}}$ results in

$$A_1^{\ 2} = k_x^{\ 2} - \omega^2\mu_1\varepsilon_1. \quad (2.19)$$

In similar fashion, the following relation is obtained from the evanescent wave propagation in the dielectric medium 2,

$$A_2^{\ 2} = k_x^{\ 2} - \omega^2\mu_2\varepsilon_2. \quad (2.20)$$

The magnetic fields of the evanescent wave in the two media, can be expressed as (Maier,2007)

$$\overrightarrow{H}_{t1}(x,z) = \frac{-j\omega\varepsilon_1\overrightarrow{E}_{t1}(x,z)}{-A_1}. \quad (2.21)$$

and

$$\overrightarrow{H}_{t2}(x,z) = \frac{-j\omega\varepsilon_2\overrightarrow{E}_{t2}(x,z)}{A_2}, \quad (2.22)$$

respectively. According to the boundary condition of the wave propagation, both tangential components of transmitted electric field and magnetic field in the two media are continuous, yielding the relationship

$$\frac{-j\omega\varepsilon_1 \vec{E}_{t1}(x,z)}{-A_1} = \frac{-j\omega\varepsilon_2 \vec{E}_{t2}(x,z)}{A_2}.$$
(2.23)

Equation (2.23) can be simplified by cancelling common factors to

$$A_1 = -\frac{\varepsilon_{r1} A_2}{\varepsilon_{r2}}.$$
(2.24)

This equation shows that the surface plasmon occurs only at the interface between two media having different signs of the relative permittivities. Substitution Eq. (2.24) to Eq. (2.19) gives

$$\left(-\frac{\varepsilon_{r1} A_2}{\varepsilon_{r2}}\right)^2 = k_x^2 - \omega^2 \mu_1 \varepsilon_1.$$
(2.25)

Consequently, the wave vector of the surface plasmon can be derived from Eq. (2.25)

$$k_x = \frac{\omega}{c}\sqrt{\frac{n_1^2 n_2^2}{n_1^2 + n_1^2}}$$
(2.26)

2.4   SURFACE PLASMON RESONANCE

In the prism-based Kretschmann configuration, the p-polarized wave incident on the gold layer is originated from the prism. Consequently, the incident wave vector is

$$k_i = n_p \omega c$$
(2.27)

where n_p is the refractive index of the prism. In terms of the incident angle, the wave vector of the evanescent wave is

$$k_x = n_p \omega c \sin \alpha_i.$$
(2.28)

Matching of the two wave vectors can be done by controlling the incident angle of the illuminating light. Since the wave-vector matching causes a resonance of the surface plasmon resonance, the incident angle α_{SPR} is defined as

$$\alpha_{SPR} = \sin^{-1}\left(\frac{1}{n_p} \sqrt{\frac{n_s^2 n_g^2}{n_s^2 + n_g^2}} \right), \qquad (2.29)$$

which also called the resonance angle.

When the surface plasmon resonance occurs, the electrons in the metal will absorb the photon energy of the incident light. As a result, a sharp dark band associated with a minimum intensity appears in the reflected light. An angle α_{SPR} is a result of detected dark band, which can then be used to evaluate the sample's refractive index by using Eq. (2.37). The SPR angle is useful for the sample detection and also for the design of SPR system components such as the suitable prism and metal for each sample.

2.5   POWELL LENS

Powell lens is also called the laser line generator (Powell, 1989). It is the lens that can convert a Gaussian-shaped laser beam into a uniform line-shaped light beam distribution. The unique shape of the Powell lens is designed to have two surfaces that are the primary surface and secondary surface. The primary surface is conic that diverges paraxial rays with a wider angle than marginal rays. The lens surface is defined by (Powell, 1989)

$$z = \frac{cy^2}{1 + \sqrt{1 - (1+Q)c^2 y^2}}, \qquad (2.30)$$

where, c and Q represent the apex curvature and the conic constant, respectively. Equation (2.30) expresses the z-component of the surface displacement at the distance y from the optical axis. Furthermore, the small curvature provides the wider fan angle and longer of uniform beam distribution. The secondary surface is a plane surface that further diverges the beam based on a simple light refraction phenomenon. Figure 2.3

(a) shows a diagram of light rays from a laser source which starts to diverge by the first surface of the Powell lens. Due to the refraction effect, the rays are transmitted from the second surface with bigger refractions angles. Figure 2.3(b) shows a 1-D cross-sectional intensity distribution transmitted by the Powell lens, which has better uniformity than a cylindrical lens.
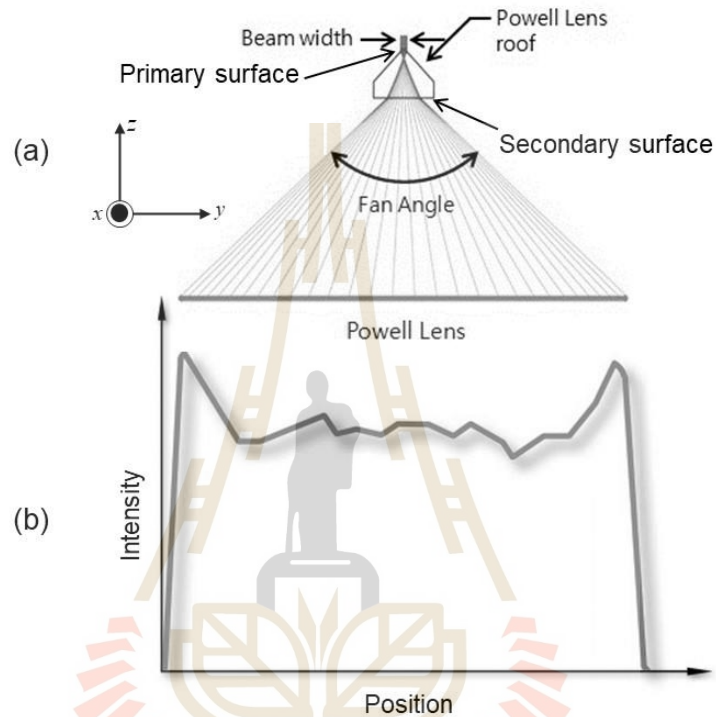
Figure 2.3 (a) Ray diagram of Powell lens and (b) the plot of 1-D
intensity distribution of the divergent beam transmitted
by the Powell lens. (http://m.s-laser.com/info/the-
requirements-of-laser-lines-for-3d-scannin-49281473.html).

2.6   REFRACTIVE INDEX OF BINARY MIXTURE

The refractive index n is a value obtained from the ratio of the speed of light in a vacuum to that in another dielectric medium. It is a fundamental property of pure liquids and their solutions (Reis et al., 2010), which depends on ambient temperature and pressure at measurement time. However, most handbooks of refractive indices list only pure substances at a particular temperature. The refractive index of the binary mixture n_m of two pure substances with refractive indices, n_1 and n_2 , can be

mathematically calculated by using Newton's theoretical rule (Gayathri et al., 2018) defined as

$$\left(n_m^2 - 1\right) = \phi_1\left(n_1^2 - 1\right) + \phi_2\left(n_2^2 - 1\right), \tag{2.31}$$

where ϕ_1 and ϕ_2 are the volume fractions of the first and second substances, respectively. They are defined as $\phi_1 = w_1 / \rho_1$ and $\phi_2 = w_2 / \rho_2$ that are the ratio of the weight w to the density of pure substance respectively.

Let consider the calculation of the refractive index of a glycerol mixture by using the Newton theory. In practice, commercially available substances have purities or concentrations stated in the unit of % volume/volume (v/v). In order to calculate a refractive index of the glycerol solution with a concentration1.0% (w/w) using the Newton theory, the volume fractions ϕ_{gly} and ϕ_w are calculated as follows. Assume the commercial glycerol has a label of the purity 99.7% (v/v) which indicates that in a 100 ml of the glycerol solution, the volume of glycerol v_{gly} is 99.7 ml and water v_w is 0.3 ml. The first step is to find masses of glycerol w_{gly} and water w_w in 100 ml solution that can be calculated as w_{gly} = 99.7 ml x ρ_{gly} (g/ml) and w_w = 0.3 ml x ρ_w (g/ml), respectively. Secondly, in order to have the concentration 1.0% (w/w) of the glycerol solution, the required mass of water $w_{w\text{-}req}$ can be calculated as

$$1\% \text{ (w/w) of glycerol solution } = \frac{w_{gly}}{w_{gly} + w_{w-req}}.$$

In terms of volume, the required volume of water $v_{w\text{-}req}$ is $m_{w\text{-}req}/\rho_w$. Hence, the weight by volume (w/v) of glycerol and water can be calculated as

$$1\% \text{ (w/v) of glycerol } = \frac{w_{gly}}{v_{gly} + v_{w-req}}$$

and

$$\text{water } = \frac{w_w}{v_{gly} + v_{w-req}},$$

respectively. Consequently, the volume fraction of glycerol is found to be

$\phi_{glycerol}$ = w_{gly}/[(v_{gly} + $v_{w\text{-}req}$)ρ_{gly}], while water is ϕ_{water} = w_w/[(v_{gly} + $v_{w\text{-}req}$)ρ_w]. The refractive index for other concentrations can be calculated by the same steps above.

CHAPTER III

RESEARCH METHODOLOGY

3.1 PROPOSED SPR SENSOR USING DIVERGENT BEAM ILLUMINATION

The optical configuration for implementing the proposed Kretschmann-based SPR sensor with a narrow divergent beam illumination is depicted in Fig. 3.1. The illuminating beam's plane of incidence is parallel to the xz plane. In the configuration, an index-matching liquid is added between the gold-evaporated glass plate and the prism to reduce multiple light refractions, and a test sample is placed on the gold plate. Φ , χ and ψ are the angles of the apex and the vertexes A and B of the prism, respectively.
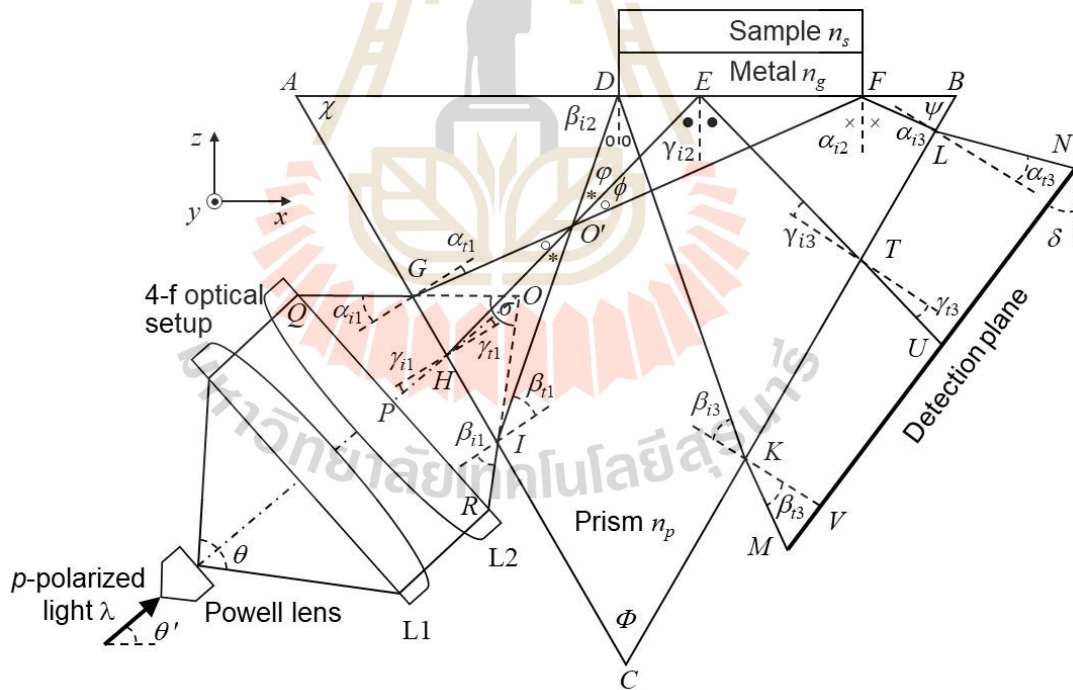
Figure 3.1 Schematic representation of the proposed SPR sensor

employing the 4f optical configuration.

In the experimental setup, a Powell lens is employed to generate a uniformly diverging line beam with an angle of divergence θ. The beam is transmitted into the prism through a 4f optical system comprised of two cylindrical lenses. The focal point of the Powell lens is aligned with the front focal plane of the first cylindrical lens, whilst the front focal plane of the second lens is positioned at the appropriate point O within the prism. However, as a result of prism refraction, the focal point changes to point O'. After light has been refracted by the prism, the rays GF and ID illuminate the prism-gold interface at angles α_{i2} and β_{i2}, respectively. These two angles correspond to the detectable variation in refractive index between n_1 and n_2, where n_2 is greater than n_1. In addition, the angle γ_{i2} is the incidence angle of the center ray HE. Note that the three angles must be larger than the prism's critical angle. The FL and DK reflected rays are refracted into the air and collected by a CMOS image sensor array. The collected SPR reflectivity pattern is then quantitatively evaluated to determine the resonance angle and the associated refractive index.

To satisfy the required resonance angles, α_{i2} and β_{i2} are defined as the incident angles, which cover all the measurement range. The divergent angle of the illuminating beam can then be determined by using triangles $\Delta DFO'$, that is

$$= \phi + \varphi = \alpha_{i2} - \beta_{i2}. \tag{3.1}$$

As a result, the laser light source has to be oriented by the angle

$$\theta' = \frac{\Phi - \alpha_{i1} + \beta_{i1}}{2} \tag{3.2}$$

with regard to the horizontal direction of an optical axis. In Eq. (3.2), α_{i1} and β_{i1} are the incident angles of the surface-transmitted rays QG and RI on the surface #AC, which can be expressed as

$$\alpha_{i1} = \sin^{-1}[n_p \sin(\chi - \alpha_{i2})] \tag{3.3}$$

and

$$\beta_{i1} = \sin^{-1}[n_p \sin(\chi - \beta_{i2})], \tag{3.4}$$

respectively. The two equations give the relationship of the incident angles at two different prism surfaces that are #AC and #AB. Besides their dependency upon the apex angle, the two angles of incidence α_{i1} and β_{i1} are determined by the transmitted divergent beam QR from the lens L2. Consequently, the widths of the beam input GI, the beam at the sensing plate DF and the beam output KL depend on the angles of incidence α_{i1} and β_{i1}. Here, the positive and the negative angles are defined as the angles formed by a clockwise and a counterclockwise rotation of the incident ray with respect to the normal line, respectively. Therefore, the optical configuration depicted in Fig. 3.1 must be aligned as follows. First, the distance PH must be less than the back focal length of the second lens. Second, the beam spot size at the focal point has to be larger than the beam width DF, which is divergent and incident at the gold sensing component on surface #AB. Without the prism, the angle QOP of the convergent beam is given by

$$\sigma = 2\tan^{-1}\left(\frac{QR/2}{BFL}\right)$$

$$= \beta_{i1} + \alpha_{i1}. \tag{3.5}$$

By placing the prism behind the lens L2 with the separation distance PH, the beam size GI that depends on the distance PH can be expressed as

$$GI = GH + HI$$

$$= \frac{BFL - PH\sin\left(\dfrac{\sigma}{2}\right)}{\cos\alpha_{i1}} + \frac{BFL - PH\sin\left(\dfrac{\sigma}{2}\right)}{\cos\beta_{i1}}. \tag{3.6}$$

After AG which is the location of the incident beam on the surface #AC is defined, the size of the divergent beam DF at the sensing plate can be calculated by

$$DF = \left(\frac{AG\cos\alpha_{t1}}{\cos\alpha_{i2}}\right) - \left[\frac{(AG + GI)\cos\beta_{t1}}{\cos\beta_{i2}}\right].$$

$$= \left\{ \frac{AG \cos\left[\sin^{-1}\left(\dfrac{\sin\alpha_{i1}}{n_p}\right)\right]}{\cos\left[\chi - \left(\dfrac{\sin\alpha_{i1}}{n_p}\right)\right]} \right\} - \left\{ \frac{(AG+GI)\cos\left[\sin^{-1}\left(\dfrac{\sin\beta_{i1}}{n_p}\right)\right]}{\cos\left[\chi - \left(\dfrac{\sin\beta_{i1}}{n_p}\right)\right]} \right\} \qquad (3.7)$$

Equation (3.7) determines the required size of the gold sensing plate for implementing the proposed SPR sensor, which has to be placed at the distance

$$AD = \frac{(AG+GI)\cos\beta_{t1}}{\cos\beta_{i2}}$$

$$= \frac{(AG+GI)\cos\left[\sin^{-1}\left(\dfrac{\sin\beta_{i1}}{n_p}\right)\right]}{\cos\left[\chi - \left(\dfrac{\sin\beta_{i1}}{n_p}\right)\right]} \qquad (3.8)$$

from the vertex A on the surface #AB of the prism.

When the diverging beam is reflected from the prism's interface with the gold layer, it becomes even more divergent. The divergent beam width KL at the surface of #BC can be expressed as

$$KL = \frac{(AB-AD)\cos\beta_{i2}}{\cos(\psi-\beta_{i2})} - \frac{(AB-AD-DF)\cos\alpha_{i2}}{\cos(\psi-\alpha_{i2})}$$

$$= \frac{(AB-AD)\cos\left[\chi - \left(\dfrac{\sin\beta_{i1}}{n_p}\right)\right]}{\cos\left[\psi - \chi + \left(\dfrac{\sin\beta_{i1}}{n_p}\right)\right]} \frac{(AB-AD-DF)\cos\left[\chi - \left(\dfrac{\sin\alpha_{i1}}{n_p}\right)\right]}{\cos\left[\psi - \chi + \left(\dfrac{\sin\alpha_{i1}}{n_p}\right)\right]}, \qquad (3.9)$$

where AB is the length of the prism hypotenuse. As a result of the prism refraction, the refracted beams KM and LN strike the sensor plane at different angles.

To achieve a uniform distribution of the incident angle of all refracted rays on the detection plane, the plane has to be tilted by the angle δ

$$\delta = 90° - \psi + \left(\frac{\beta_{t3} + \alpha_{t3}}{2}\right)$$

$$= 90^\circ - \psi + \left(\frac{\beta_{i1} + \alpha_{i1}}{2} \right). \tag{3.10}$$

with respect to the vertical axis. Here, α_{t3} and β_{t3} are equal to the angles α_{i1} and β_{i1}, respectively. By aligning the first and last pixels of the image sensor with the rays *KM* and *LN*, respectively, the whole SPR reflectivity pattern may be captured by utilizing the full width *MN* of the image sensor. The alignment requires the distance of separation

$$KV = \frac{\left[\dfrac{MN \cos\left(\dfrac{\alpha_{t3} - \beta_{t3}}{2} \right) - KL \cos\alpha_{t3}}{\sin(\beta_{t3} - \alpha_{t3})} \right] \cos\left(\dfrac{\alpha_{t3} - \beta_{t3}}{2} \right)}{\cos\left(\dfrac{\beta_{t3} + \alpha_{t3}}{2} \right)}$$

$$= \frac{\left[\dfrac{MN \cos\left(\dfrac{\alpha_{i1} - \beta_{i1}}{2} \right) - KL \cos\alpha_{i1}}{\sin(\beta_{i1} - \alpha_{i1})} \right] \cos\left(\dfrac{\alpha_{i1} - \beta_{i1}}{2} \right)}{\cos\left(\dfrac{\beta_{i1} + \alpha_{i1}}{2} \right)} \tag{3.11}$$

with respect to the prism. In contrast, the separation distance *KV* can be used to compute the needed sensor width. In this situation, the width of the sensor is found to be

$$MN = \frac{\left[\dfrac{KV \sin(\beta_{t3} - \alpha_{t3}) \cos\left(\dfrac{\beta_{t3} + \alpha_{t3}}{2} \right)}{\cos\left(\dfrac{\alpha_{t3} - \beta_{t3}}{2} \right)} \right] + KL \sin(90^\circ + \alpha_{t3})}{\cos\left(\dfrac{\alpha_{t3} - \beta_{t3}}{2} \right)}$$

$$= \frac{\left[\dfrac{KV \sin(\beta_{i1} - \alpha_{i1}) \cos\left(\dfrac{\beta_{i1} + \alpha_{i1}}{2}\right)}{\cos\left(\dfrac{\alpha_{i1} - \beta_{i1}}{2}\right)} \right] + KL \sin(90° + \alpha_{i1})}{\cos\left(\dfrac{\alpha_{i1} - \beta_{i1}}{2}\right)} . \qquad (3.12)$$

Equation (3.11) provides the condition for the complete use of the image sensor's known width *MN*, whereas Equation (3.12), for a given separation distance *KV*, specifies the criteria for choosing the image sensor. Since the width of the reflected beam *KL* is known, it is possible to determine the pixel position of the SPR dip intensity, producing measurements of the resonance angle and the corresponding refractive index.

3.2   DESIGN OF THE PROPOSED SENSOR

Consider that the proposed sensor will be used for measuring refractive indices of liquids with variation from 1.0462 to 1.3841. When the sensor is implemented by using an equilateral prism fabricated from N-SF11 (n_p = 1.785) and a gold layer (n_g = 0.1728+j3.4218) (Yamamoto, 2002), Eq. (2.29) gives their corresponding resonance angles of 38° and 58°, which define the range of the angles β_{i2} and α_{i2} of the divergent beam incident on the gold sensing plate *DF*, respectively. The divergent beam is produced by the 4f optical setup which has the back focal length BFL equals to 17.74 mm and the beam size *QR* is equal to 12.3 mm. According to the specifications of the optical components, it provides the incident angles at the surface #*AC* equal to β_{i1} = 41.96° to α_{i1} = -3.57°. Without the prism, the angle σ of the convergent beam is 38°. Consequently, the illuminating light needs to be oriented at the angle θ' = 53°, while the orientation angle δ of the sensor plane is 40°. Furthermore, the size of the beam *GI* incident on the prism that depends on the distance *PH* can be calculated by using Eq. (3.5). In order to detect the whole SPR reflectivity signals, the distance *FB*, *BL*, and *KC* must be greater than zero. This condition can be satisfied, provided that the suitable distance *PH* and incident position *AG* are determined.

Table 3.1 Beam sizes *GI, AG, DF, KL* and *MN* as a function of the illumination distance *PH* for β_{i1} = 41.96°, α_{i1} = -3.57° and *QR* = 12.3 mm.

PH (cm)	GI (mm)	AG (mm)		DF (mm)		KL (mm)	MN (mm)
		min	max	min	max		
1.4	2.9	6.5	7.5	1.2	1.9	1.9	38.0
1.5	2.1	5.5	7.5	1.4	2.8	2.7	38.8
1.6	1.3	4.0	7.5	1.3	3.7	3.5	39.6

Table 3.1 shows the beam sizes on different prism surfaces and the sensor as a function of the distance *PH*. They are calculated by using the equations derived in the previous section. In order to be experimentally realizable, the distance *PH* was varied by 1 mm, giving the size of the beam *GI*. It is apparent that due to the fixed shape of the illuminating divergent beam, the beam size *GI* incident on the prism becomes smaller as the distance *PH* increases. Consequently, the smaller the beam size *GI* the broader the range of the incident beam position *AG*. As a result, the gold plate with the size *DF* and the position *AD* can be obtained by using Eqs. (3.7) and (3.8) as a function of the possible incident position *AG*, respectively.

Next, the resultant beam size *KL* on the prism exit surface can be calculated by using Eq. (3.9). By taking the size of commercially available CMOS sensors into account, the distance *KV* is set to 56 mm. Consequently, the output beam pattern that maps the incident beam with the angle range of β_{i1} = 41.96° to α_{i1} = -3.57° can be detected by using the sensor with the size of *MN* defined as Eq. (3.12). The values of *KL* and *MN* are presented in the last two columns in Table 3.1. In summary, the longer the distance *PH*, the larger the beam sizes *DF* and *KL*. The table can be used as guidelines for designing the SPR setup.
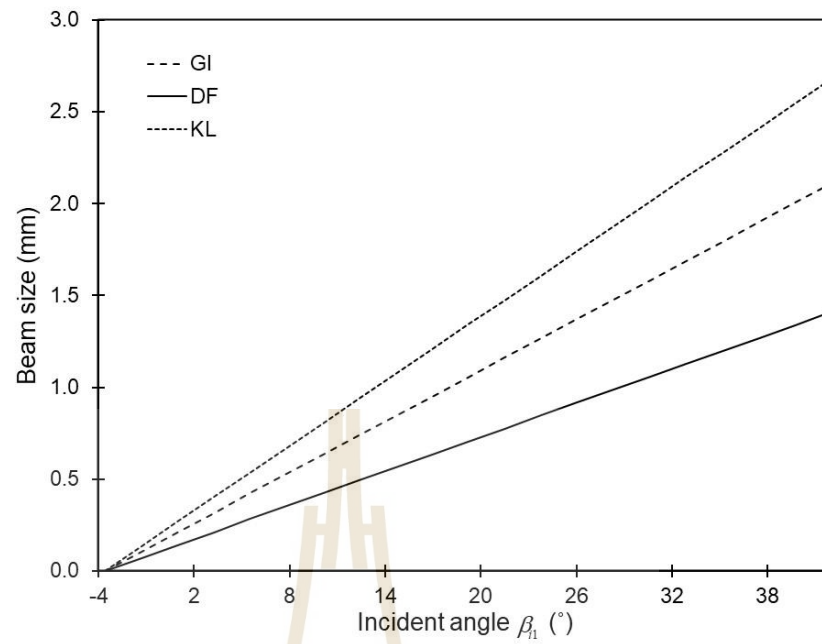
Figure 3.2 Plots of the beam sizes *GI, DF* and *KL* as a function of

the incidence angle β_{i1}.
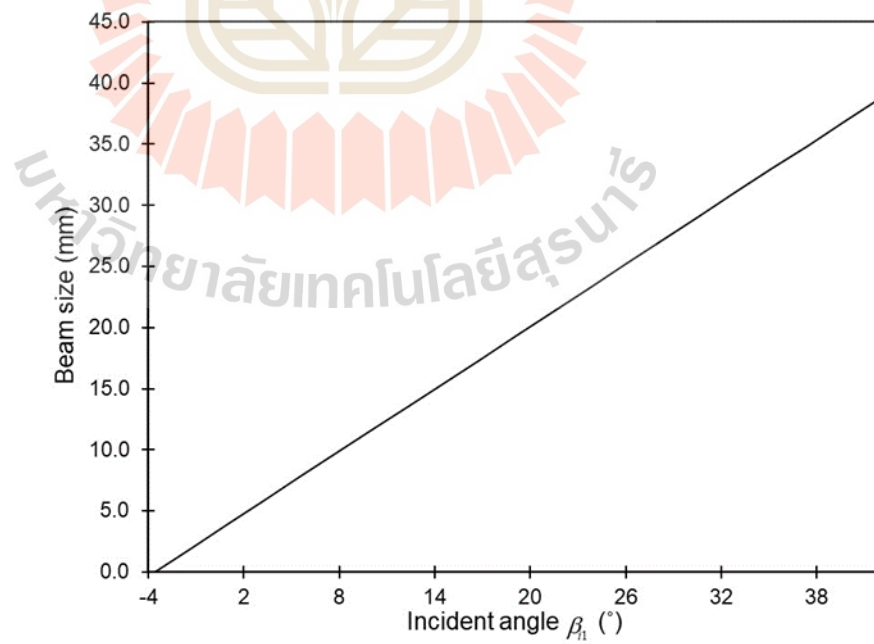
Figure 3.3 Plots of the beam size at the detection plane *MN* as

a function of the incidence angle β_{i1}.

According to Table 3.1, this resonance sensing could be implemented by setting the separation distance *PH* to 15 mm and the incident beam position *AG* of 5.5 mm. They caused the beams *GI*, *DF*, *KL* and *MN* became equal to 2.1 mm, 1.4 mm, 2.7 mm and 38.8 mm, respectively. Figure 3.2 and 3.3 shows the variations of the beam size *GI*, *DF*, *KL* and *MN* as a function of the angle of incidence β_{i1}. Since the angle of the incident beam *DF* varies from β_{i2} to α_{i2}, the graph in Fig. 3.2 and 3.3 will also vary the beam as a function of the angle of incidence β_{i1} to α_{i1}. The beam sizes inside and outside the prism linearly increase as the incident angle β_{i1} becomes bigger. Therefore, the designed SPR sensor could linearly distribute the beams on the interface of the gold sensing plate and the detector plane as a function of the incident angle α_{i1}. This is important for the detection of the SPR reflectivity curve recorded by using the array sensor.
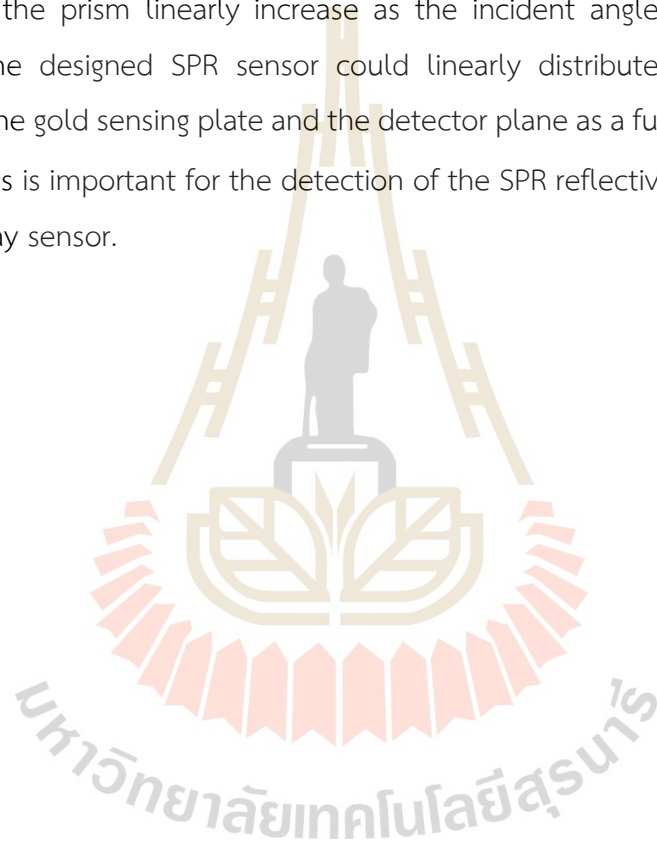
CHAPTER IV

EXPERIMENTAL VERIFICATIONS

4.1 GLYCEROL SOLUTIONS FOR SENSING VERIFICATIONS

In order to demonstrate the viability of the proposed methodology, several concentrations of glycerol (n_{gly} = 1.4707) (Rheims et al., 1997) were measured experimentally at 25° C using the proposed SPR apparatus depicted in Fig. 4.1. The use of glycerol as a solution sample was because it is non-toxic (Becker et al., 2019) and hard to evaporate at room temperature (Yong et al., 2017). On the basis of the Newton theoretical rule (Gayathri et al., 2018), the concentrations of glycerol varied from 1 – 10% weight per weight (w/w) by diluting with water (n_w = 1.3317) (Hale et al., 1973).

Table 4.1 Refractive index and resonance angle calculated as a function of glycerol concentration.

Glycerol Concentration (%)	Refractive Index n_s	Resonance Angle (°)
0	1.3317	54.104
1	1.3329	54.189
2	1.3340	54.266
3	1.3352	54.351
4	1.3364	54.435
5	1.3375	54.513
6	1.3387	54.599
7	1.3399	54.684
8	1.3410	54.763
9	1.3423	54.856
10	1.3435	54.942

The computed refractive index is displayed in Table 4.1 as a function of the glycerol concentration. It is evident that the refractive index varies linearly with the concentration change by a mean interval of approximately 0.0012. The final column of Table 1 displays the calculated resonance angle using Eq. (2.29). The Abbe refractometer (Atago, 1220 NAR-2T) with a measuring range of 1.3000 to 1.7000 and resolution of 0.001 RIU was used to measure the refractive index compared to the proposed SPR sensor to verify the accuracy and credibility. The experimental measurements of the refractive index were done on three sets of samples. Each concentration was repeatedly measured ten times.

4.2   EXPERIMENTAL SETUP
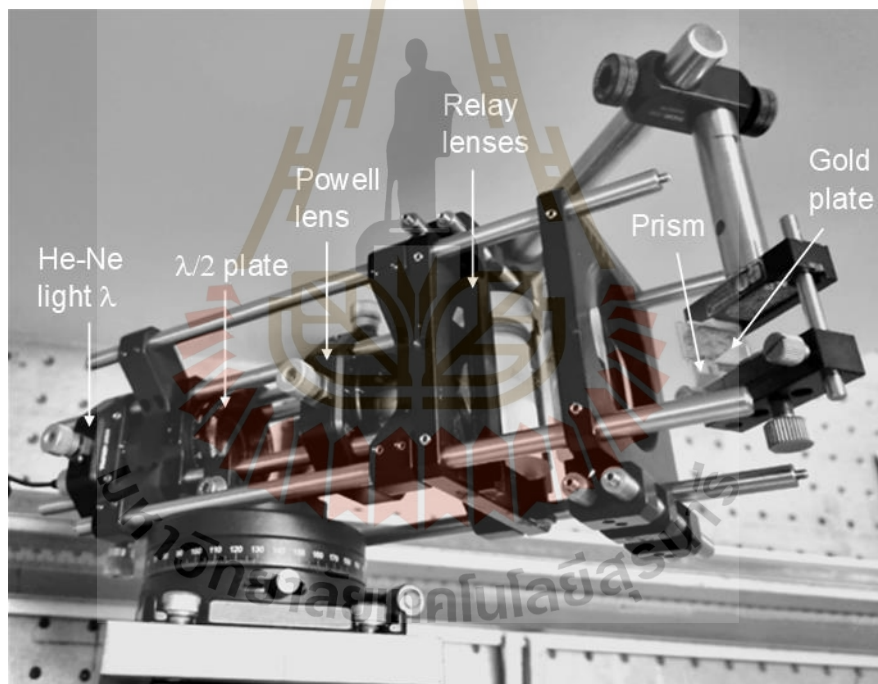
Figure 4.1 The experimental verification setup for the proposed
divergent-beam-based SPR sensor.

Figure 4.1 shows the optical setup for the experimental verification of the proposed method. The plasmon resonance was produced by sandwiching a gold-evaporated glass plate (Nano SPR, BA1000) with a refractive index of n_g = 0.1728+j3.4218 (Yamamoto, 2002) between the sample and a 15 mm N-SF11

equilateral prism (n_p = 1.785) (Edmunds, #49-432). The index matching liquid (Series A; Cargille-Sacher Laboratories, Inc.) was used to fill the space between the prism and the gold plate. A laser light source with wavelength equals to 635 nm (Thorlabs, #CPS635) was passed through a half-wave plate (Thorlabs, #WPH10E-633) to produce a p-polarized beam. The optical axis of the illuminating light was fixed at the angle θ' = 53°. After passing through a Powell lens with a 45° fan angle (Thorlabs, #PL0145), the 4f optical relay configuration with a 25 mm focal length focused the uniformly diverging beam on point *O*. The *AG* and *PH* distances were set to 5.5 mm and 15 mm, respectively. However, as a result of prism refraction, the focusing point was relocated to point *O'* and the divergent beam incident on the sensing region had angles ranging from 38° to 58°, which are equal to β_{i1} = 41.96° to α_{i1} = -3.57° as mentioned in section 3.2. In order to measure the refractive index of each glycerol concentration, the CMOS sensor (Basler, daA2500-14um) with 2592 pixel × 1944 pixel in an area of 5.7 mm × 4.3 mm was tilted in relation to the vertical axis by an angle δ of approximately 40°. The distance *KV* was adjusted at 56 mm, whereas *MV* was 12.5 mm.

4.3 UNIFORM DIVERGENT BEAM USING POWELL LENS
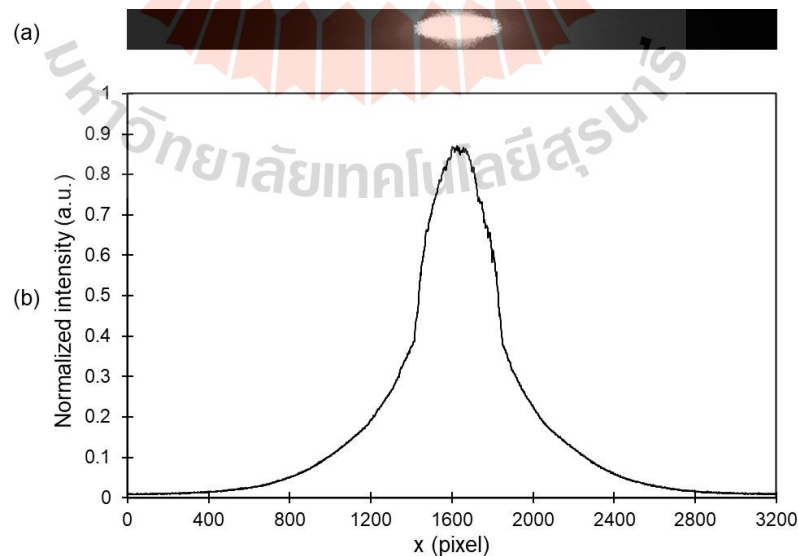
Figure 4.2 The divergent beam generated by using the cylindrical lens and
(b) its intensity scanned along the horizontal direction.
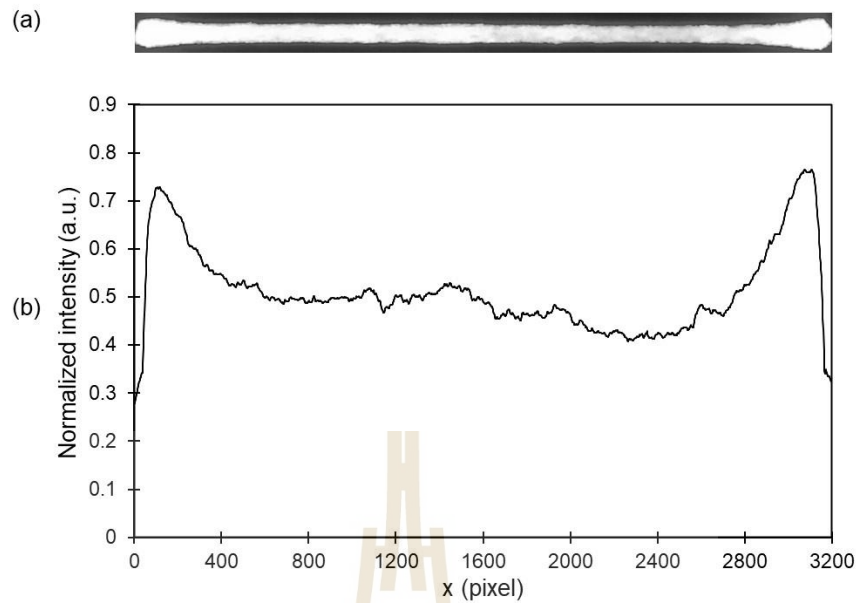
Figure 4.3 The divergent beam generated by using the Powell lens and
(b) its intensity scanned along the horizontal direction.

As discussed in section 2.5, the Powell lens was used to generate the uniform divergent beam illumination. In order to understand the advantage of the Powell lens compared to the cylindrical lens, their beam outputs are compared as follows. Figure 4.2 (a) shows the intensity pattern of the divergent beam generated by using a cylindrical lens. The beam was recorded at a distance of 16 cm behind the lens, while the laser source was 14 cm in front of the lens. Figure 4.2 (b) plots its intensity scanned along the horizontal axis. It is apparent that the beam intensity profile is localized around its origin. This is because a laser beam has an inherently Gaussian electric field profile. When the beam is used for the illumination of the SPR sensor, the dip intensity of SPR reflectance may be degraded by the Gaussian distribution nature of the laser beam. Figure 4.3 (a) shows the intensity pattern of the divergent beam generated by using the Powell lens by using the same laser illumination setup. The beam was recorded at the distance of 6 cm behind the lens. It is obvious that the Gaussian beam profile is eliminated. Besides having better uniformity, the divergent beam becomes broader because of the conic surface of the Powell lens. In the plots, the scanned intensities were normalized by the maximum intensity of the laser source.

4.4   VALIDATION OF THE SETUP

To verify the alignment of the experimental setup, the beam sizes at different parts of the setup were estimated by using the millimeter paper graph. The estimated beam sizes were shown in Table 4.2.

Table 4.2 The beam sizes at different parts of the setup with the distances
PH = 15 mm, AG = 5.5 mm, β_{i1} = 41.96° to α_{i1} = -3.57°.

Beam size	Theory (mm)	Estimation (mm)	% Error
BFL	17.74	18	1.5
QR	12.35	12	2.8
GI	2.11	2	5.2
DF	1.41	2	42
KL	2.68	3	12

4.5   DETECTION OF SPR DIP INTENSITY
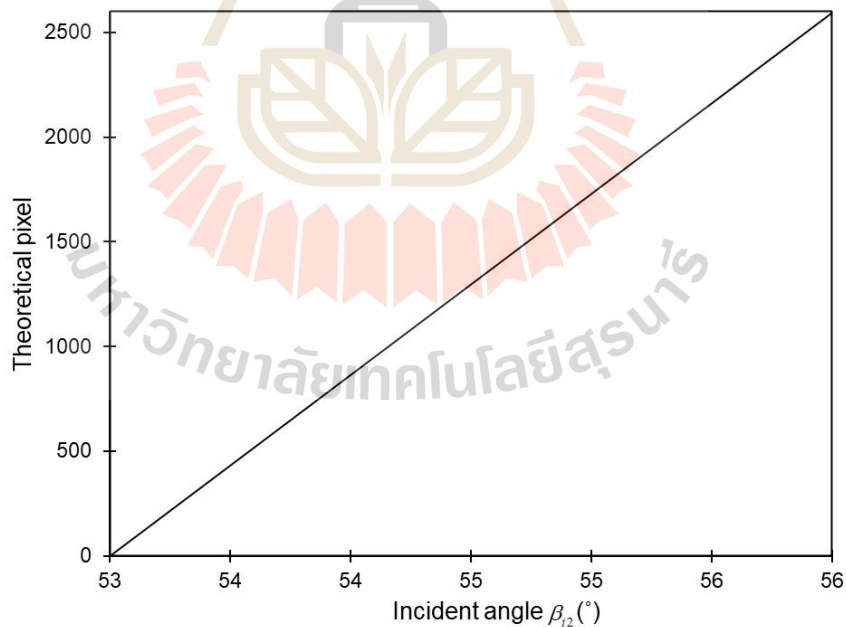
Figure 4.4 Plots of the number of pixel as a function of the incidence angle β_{i2}.

In order to measure the refractive index of the glycerol solutions, the relationship between the angle of incidence of the light rays in the gold sensing chip *DF* and the pixel of the array sensor with the size *MN* is determined by

$$\text{Detected pixel} = \frac{\left(\dfrac{MN}{\text{pixel size}}\right) \times (\alpha_{SPR} - \beta_{i2})}{\beta_{i2} - \alpha_{i2}}. \tag{4.1}$$

where β_{i2} and α_{i2} are the range of the sample resonance angle that can be measured. In the case of the measurement of the samples in Table 4.1, the angles β_{i2} and α_{i2} were set to be equal to 53° and 56°, respectively. To detect the SPR dip intensity using the Basler image sensor, the sensor was aligned in such a way that the first and 2592th pixels detected the light rays with the angle of incidences of 53° and 56°, respectively. Figure 4.4 shows the theoretical relationship between the pixel position of the SPR dip intensity detected at the Basler image sensor as a function of the incident angle β_{i2}. After the SPR angle is obtained by detecting the dip intensity, it can be used to find the refractive index of the sample. In comparison with curve fitting in Appendix A, the detection of the minimum dip intensity gives better accuracy.

4.6   MEASUREMENT OF GLYCEROL'S REFRACTIVE INDEX
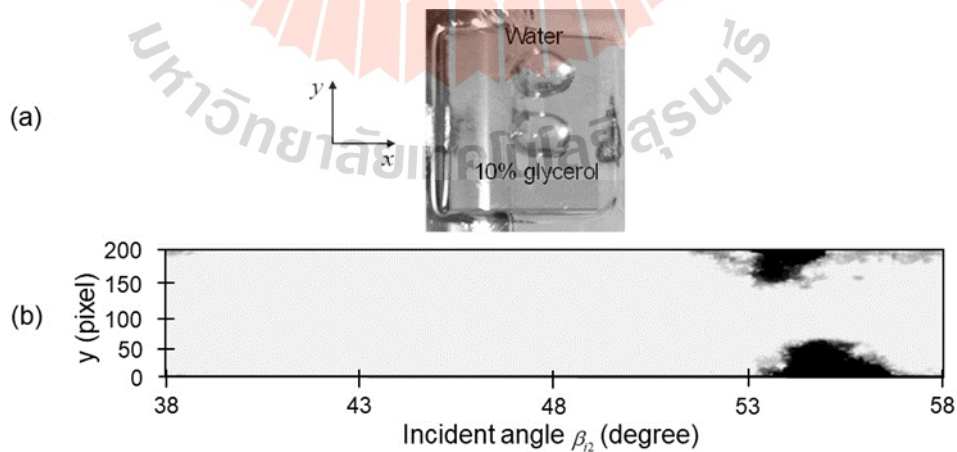
Figure 4.5 (a) Droplets of water and 10% glycerol above the gold plate and
(b) the corresponding SPR reflectivity pattern by using p-polarized
light.

In order to minimize measurement errors, each glycerol sample was tested concurrently with a calibrating sample of water. Figure 4.5 (a) depicts two droplets of water and 10% glycerol solution placed next to one another on the *y*-axis of a gold plate with a 10-microliter pipette (Brandtech, Transferpette S Pipette). The alignment of the samples along the y-axis reveals that the proposed arrangement is suitable for multichannel measurements. Figure 4.5 (b) depicts the pattern of SPR reflectivity matching the samples. The *x* and *y*-axis of the captured pattern correspond to the horizontal and vertical directions of light distribution on the gold plate.
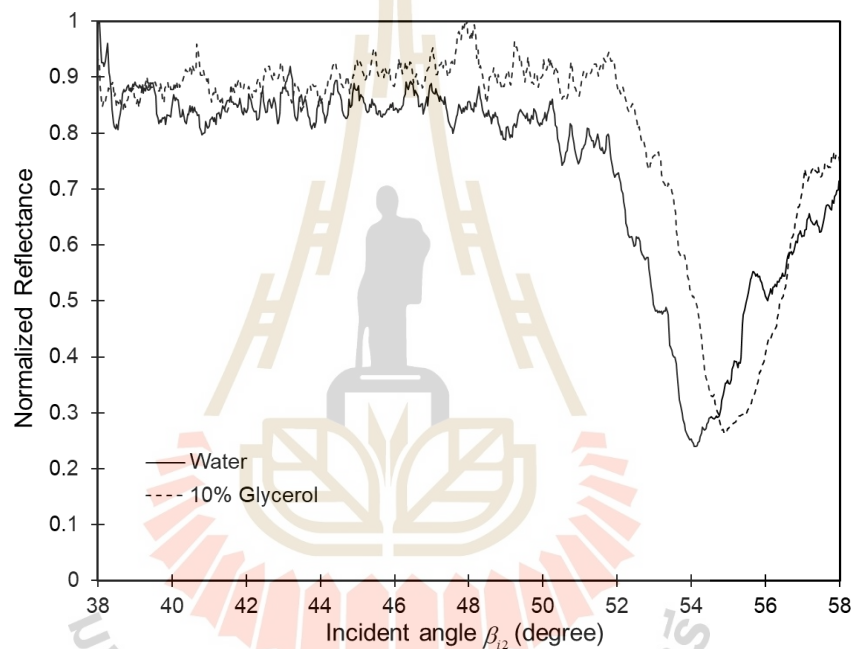
Figure 4.6 The average SPR reflectivity pattern of water and 10% glycerol
along the vertical direction of Fig. 4.5.

Figure 4.6 illustrates the cross-sectional SPR reflectivity of the water and glycerol solutions depicted in Fig. 4.5 (b). Each reflectivity scan provides an average vertical intensity of fifty pixels. The SPR reflectivity dip intensities of water and glycerol appear at around 54° and 55°, respectively. Due to its greater refractive index, glycerol's reflectivity curve is kind of wider than that of water. The results of the experiment validated the viability of the proposed method for single-shot measurement of multichannel refractive index.
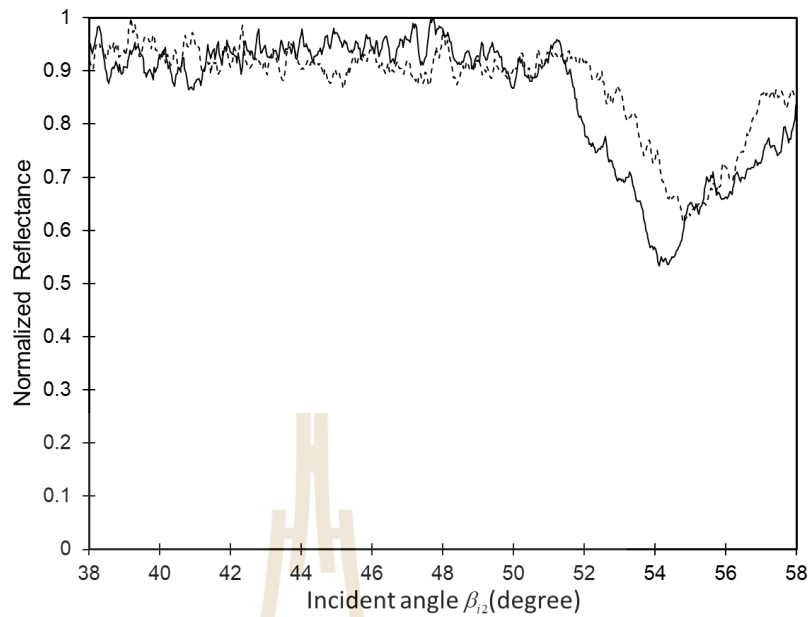
Figure 4.7 The average SPR reflectivity pattern of water and 10% glycerol
along the vertical direction was measured by using p+s polarized
light.

Figure 4.7 plots the SPR reflectivity pattern of water and 10% glycerol solution
obtained by using p+s polarized light. This polarized light was generated by rotating
the half-wave plate by 22.5°. When this polarized light was used for the illumination,
the s-polarized wave was totally reflected, distorting the reflectivity caused by the p-
polarized light. The dip minimum intensity became shallow and appeared at a wrong
angle. It can also show the SPR angle of water and 10% glycerol but it is not accurate
as the graph in Fig. 4.6.
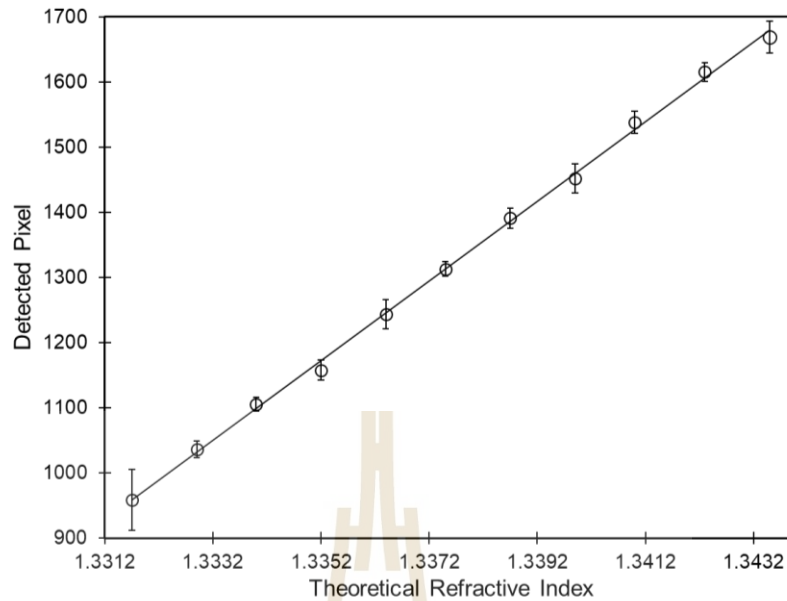
Figure 4.8 Average positions of the experimentally detected dip intensity
and their SDs as a function of the refractive index.

As mentioned in Table 4.1, Figure 4.8 displays the average position of the experimentally detected SPR dips as a function of the sample refractive index with the standard derivation appear as bar in the graph. The circle indicates the average dip position, whereas the solid line is the best-fitting linear regression line $y = 61067x-80364$. The calculated coefficient of determination R^2 gives 0.99896. This implies that there is a positive linear relationship between the intensity position of the recorded dip and the increase in the sample's refractive index. The SD shows that the measurements are closely localized around the average positions of the detected pixels (see Appendix B). Therefore, the proposed SPR system is reliable. As determined by the regression line, the sensitivity of the proposed sensor is 1.6375×10^{-5} RIU/pixel. In terms of the angle, the angular sensitivity can be expressed as

$$\text{Angular Sensitivity} = \frac{\text{Range of measurement angle}}{\text{Number of image sensor pixel} \times \text{Sensitivity (RIU/pixel)}}$$

$$= \frac{3°}{2592 \text{ pixel} \times 1.6375 \times 10^{-5} \text{ RIU/pixel}}$$

$$= 70.681° \text{/RIU}$$

which is higher than the previous method (Widjaja et al., 2021). According to Homola (Homola et al., 1999), the proposed system has a theoretical sensitivity of approximately 70.089°/RIU. Consequently, the entire length of the sensor can detect the light beam incident on the gold plate at an angle between 53° to 56° on the gold plate, yielding the angular resolution of 0.00116°/pixel, as calculated by

$$\text{Angular Resolution} = \text{Angular Sensitivity (}^\circ\text{/RIU)} \times \text{Sensitivity (RIU/pixel)}$$
$$= 70.681 \ (^\circ\text{/RIU}) \times 1.6375 \times 10^{-5} \ (\text{RIU/pixel})$$
$$= 0.00116^\circ\text{/pixel}.$$

The resolution of the proposed method is approximately 2.5 times better than the previous divergent beam-based SPR sensor, which had a resolution of 0.00289° (Widjaja et al., 2021). After averaging the detected dip places, the resulting value was utilized to calculate the resonance angle. Finally, the sample's refractive index was determined by solving Eq (2.29).

Table 4.3 The mean absolute errors by using the proposed methodology and the refractometer, the ten samples were measured for their resonance angles and refractive index.

Glycerol concn (%)	Theory		Refractometer		Proposed Method			
	RI	α_{SPR} ($^\circ$)	RI	% Error	α_{SPR} ($^\circ$)	% Error	RI	% Error
0	1.3317	54.104	1.3318	0.008	54.110	0.01	1.3318	0.008
1	1.3329	54.189	1.3331	0.02	54.201	0.022	1.3331	0.02
2	1.3340	54.266	1.3342	0.01	54.280	0.026	1.3342	0.01
3	1.3352	54.351	1.3354	0.01	54.340	0.020	1.3351	0.007
4	1.3364	54.435	1.3363	0.007	54.440	0.007	1.3364	0.00
5	1.3375	54.513	1.3380	0.04	54.519	0.01	1.3376	0.007
6	1.3387	54.599	1.3390	0.02	54.610	0.020	1.3389	0.01
7	1.3399	54.684	1.3403	0.03	54.681	0.005	1.3399	0.00
8	1.3410	54.763	1.3413	0.02	54.780	0.031	1.3412	0.01

Table 4.3 The mean absolute errors by using the proposed methodology and the
refractometer, the ten samples were measured for their resonance angles
and refractive index. (Continued)

Glycerol concn (%)	Theory		Refractometer		Proposed Method			
	RI	α_{SPR} (o)	RI	% Error	α_{SPR} (o)	% Error	RI	% Error
9	1.3423	54.856	1.3430	0.05	54.871	0.027	1.3425	0.01
10	1.3435	54.942	1.3442	0.05	54.931	0.020	1.3434	0.007

The mean absolute errors in measurements of sample refractive indices and corresponding resonance angles using the proposed method and refractometer are displayed in Table 4.3. In the table, RI represents the refractive index, whilst the resonance angles were derived using the experimentally determined position of the dip intensities. Using the proposed method and the refractometer, the mean absolute errors in measuring the refractive index of varied glycerol concentrations tend to be less than 0.1%. It is essential to remark that the overall errors of the suggested method never exceed those of the refractometer. In conclusion, the experimental findings confirm the dependability and validity of the suggested divergent beam generation within the prism for deploying SPR sensors.

CHAPTER V

CONCLUSIONS

5.1   CONCLUSIONS

This thesis has proposed and experimentally verified a new method for enhancing the SPR sensitivity using a small divergent beam illumination inside the prism via the optical relay setup. In comparison with the conventional 3-layer SPR sensors, the proposed SPR system can be implemented by using a commercial array image sensor without any mechanical movements. Experimental verification of the proposed method was done by simultaneously measuring two channels of the glycerol refractive index with different concentrations from 0 to 10 % w/w.

The experimental results show that :

- The thesis has proposed and experimentally verified the compact and low-cost SPR sensing system by using a commercially available CMOS image sensor and without mechanical scanning.

- The proposed SPR system can be implemented for multichannel sensors.

- The proposed method could improve the SPR angular resolution to about 1.16 mdeg/pixel and sensitivity to about 1.6375×10^{-5} RIU/pixel or 70.681°/RIU.

- The mean absolute errors in measuring the refractive index of various glycerol concentrations tend to be less than 0.1%.

5.2   FUTURE WORK

This thesis has accomplished the goals of reducing beam output size and increasing the sensitivity. In future work, the proposed method will be applied to bacteria and gas detection.

REFERENCES

Bak, S., Kim, G. H., Jang, H., Kim, J., Lee, J., Kim, C. S. (2018). Real-time SPR imaging based on a large area beam from a wavelength-swept laser. *Opt. Lett.,* 43 (21)*,* 5476-5479.

Becker, L.C., Bergfeld, W.F., Belsito, D.V. (2019). Safety Assessment of Glycerin as Used in Cosmetics. International Journal of Toxicology., 38 (3), 6-22.

Chan, B.L., Jutamulia, S. (2014). Micro-prism test chip. *US Patent Application Number,* 14/120,049

Chen, R., Wang, M., Wang, S., Liang, H., Hu, X., Sun, X. (2015). A low-cost surface plasmon resonance biosensor using a laser line generator. *Opt. Commun.,* 349, 83-88.

Chinowsky, T.M., Quinn, J.G., Bartholomew, D.U., Kaiser, R., Elkind, J.L. (2003). Performance of the Spreeta 2000 integrated surface plasmon resonance affinity sensor. *Sens. Actuators B Chem.,* 91 (1–3), 266-274.

Daimon, M., Masumura, A. (2007). Measurement of the refractive index of distilled water from the near-infrared region to the ultraviolet region. *Appl. Opt.,* 46, 3811-3820

Fathi, F., Jalili, R., Amjadi, M., Rashidi, M. R. (2019). SPR signals enhancement by gold nanorods for cell surface marker detection. *BioImpacts,* 9 (2), 71-78.

Firdous, S., Anwar, S., Rafya, R. (2018). Development of surface plasmon resonance (SPR) biosensors for use in the diagnostics of malignant and infectious diseases. *Laser Phys. Lett.,* 15 (6), 65602-65607.

Gayathri, A., Venugopal, T., Padmanaban, R. (2018). A comparative study of experimental and theoretical refractive index of binary liquid mixtures using mathematical methods. *IOP Conf. Series: Mater. Sci. Eng.,* 390, 1-4.

Guoqiang, L., Yachen, G. (2018). Surface plasmon resonance sensor with high sensitivity and wide dynamic range. *IEEE Sens. J.,* 18 (13), 5329-5333.

Hale, G. M., Querry, M. R. (1973). Optical constants of water in the 200-nm to 200-µm wavelength region. *Appl. Opt.,* 12, 555-563.

Haynes, W. M., Lide D. R., Bruno, T. J. (2014). CRC Handbook of Chemistry and Physics. Hoboken: CRC Press.

Herminjard, S., Sirigu, L., (2009). Surface plasmon resonance sensor showing enhanced sensitivity for CO_2 detection in the mid-infrared range. *Opt. Exp.,* 17 (1), 293-303.

Homola, J., Koudela, I., Yee, S.S. (1999). Surface plasmon resonance sensors based on diffraction gratings and prism couples: sensitivity comparison. *Sens. Actuators B Chem.,* 54 (1-2), 16-24.

Hu, J., Cao, B., Wang, S., Li, J., Wei, W., Zhao, Y., Hu, X., Zhu, J., Jiang, M., Sun, X., Chen, R., Ma, L. (2016). Design and fabrication of an angle-scanning based platform for the construction of surface plasmon resonance biosensor. *Opt. Lasers Eng.,* 78, 1-7.

Isaacs S., Abdulhalim I. (2015). Long range surface plasmon resonance with ultra-high penetration depth for self-referenced sensing and ultra-low detection limit using diverging beam approach. *Appl. Phys. Lett.,* 106 (19), 193701.

Kabashin, A. V., Patskovsky, S., Grigorenko, A. N. (2009). Phase and amplitude sensitivities in surface plasmon resonance bio and chemical sensing. *Opt. Exp.,* 17, 21191-21204.

Ke, H., Du, X., Wang, L. (2020). Detection of morphine in urine based on a surface plasmon resonance imaging immunoassay. *Anal. Methods,* 12, 3038-3044.

Kodoyianni, V. (2011). Label-free analysis of biomolecular interactions using SPR imaging. *BioTechniques,* 50 (1), 32-40.

Lan, G., Li, S., Ma, Y. (2015). Sensitivity and figure-of merit enhancements of liquid-prism SPR sensor in the angular interrogation. *Opt. Commun.,* 352, 49-54.

Li, X., Shu, J., Gu, W., Gao, L. (2019). Deep neural network for plasmonic sensor modeling. *Opt. Mater. Express,* 9, 3857-3862.

Liu, Q., Yuan, H., Liu, Y., Wang, J., Jing, Z., Peng, W. (2018). Real-time biodetection using a smartphone-based dual-color surface plasmon resonance sensor. *J. Biomed. Opt.,* 23 (4), 1–6.

Maier, S. A. (2007). Plasmonics: Fundamentals and applications. New York: Springer.

Mudgal, N., Saharia, A. (2020). Modeling of highly sensitive surface plasmon resonance (SPR) sensor for urine glucose detection. *Opt. Quantum Electron.,* 52, 1-14.

Patskovsky, S., Meunier, M. (2013). Integrated Si-based nanoplasmonic sensor with phase-sensitive angular interrogation. *Ann. Phys.,* 525 (6), 431-436.

Pérez-Ocón, F., Pozo, A.M., Cortina, J., Rabaza, O. (2021). Surface plasmon resonance sensor of CO_2 for indoors and outdoors. *Appl. Sci.,* 11, 6869-6877.

Powell, I. (1989). Linear Diverging Lens. *US Patent*, US4826299 (A) 2.

Puiu, M., Bala, C. (2016). SPR and SPR Imaging: recent trends in developing nanodevices for detection and real-time monitoring of biomolecular events. *Sensors,* 16 (6), 870-884.

Reis, J. C., Lampreia, I. M., Santos, A. F., Moita, M. L., & Douheret, G. (2010). Refractive index of liquid mixtures: theory and experiment. *Chemphyschem*, 11(17), 3722-3733.

Rheims, J., Köser, J., Wriedt, T. (1997). Refractive-index measurements in the near-IR using an Abbe refractometer. *Meas. Sci. Technol.,* 8 (6), 601-605.

Ruemmele, J. A., Golden, M. S. (2008). Quantitative surface plasmon resonance imaging: A simple approach to automated angle scanning. *Anal. Chem.,* 80 (12), 4752-4756.

Schasfoort (Ed.), R. B. M. (2017). Handbook of surface plasmon resonance. Croydon: The Royal Society of Chemistry.

Su, Y.-Y., Marsh, A., Haddrell, A. E., Li, Z.-M., Reid, J. P. (2017). Evaporation Kinetics of Polyol Droplets: Determination of Evaporation Coefficients and Diffusion Constants. Journal of Geophysical Research: Atmospheres, 122 (22), 12,317-312,334.

Szymanska, B., Lukaszewski, Z., Zelazowska-Rutkowska, B., Hermanowicz-Szamatowicz, K., Gorodkiewicz, E. (2021). An SPRi biosensor for determination of the ovarian cancer marker HE4 in human plasma. *Sensors,* 21 (10), 3567-3575.

Tang, Y., Zeng, X., Liang, J. (2010). Surface plasmon resonance: an introduction to a surface spectroscopy technique. *J. Chem. Educ.,* 87, 742-746.

Thadson, K., Visitsattapongse, S., Pechprasarn, S. (2021). Deep learning-based single-shot phase retrieval algorithm for surface plasmon resonance microscope based refractive index sensing application. *Sci. Rep.,* 11, 16289-16289.

Wang, J., Smith, R. (2014). Highly sensitive multipoint real time kinetic detection of Surface plasmon bioana- lytes with custom CMOS camera. *Biosens. Bioelectron.,* 58, 157-164.

Widjaja, J., Hossea, J. (2021). Experimental validations of divergent beam illumination and detection conditions in a surface plasmon resonance sensor using a Powell lens. *Lasers Eng.,* 48 (1-3), 17-32.

Yamamoto, M. (2002). Surface Plasmon Resonance (SPR) Theory: Tutorial. *Rev. Polarogr,* 48 (3), 209-237.
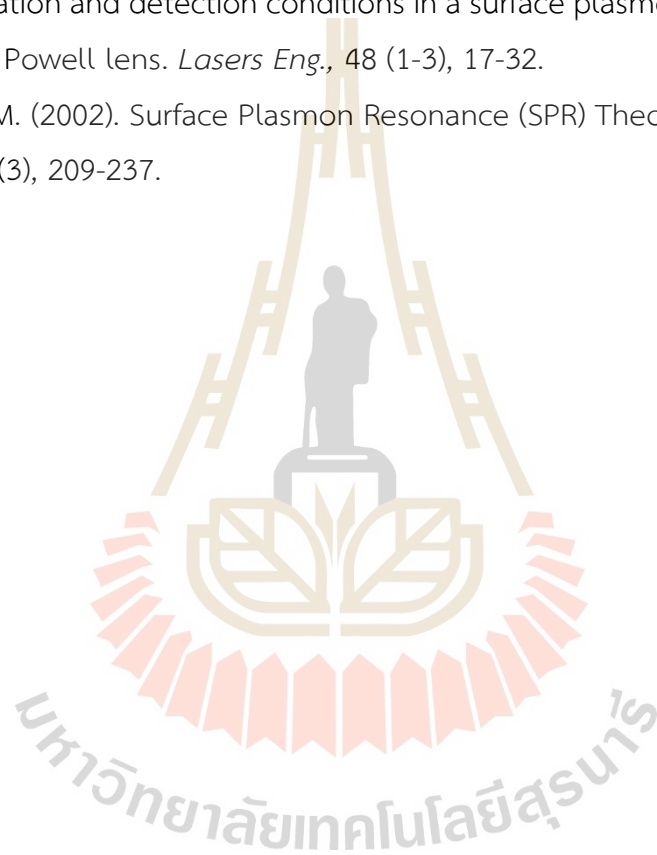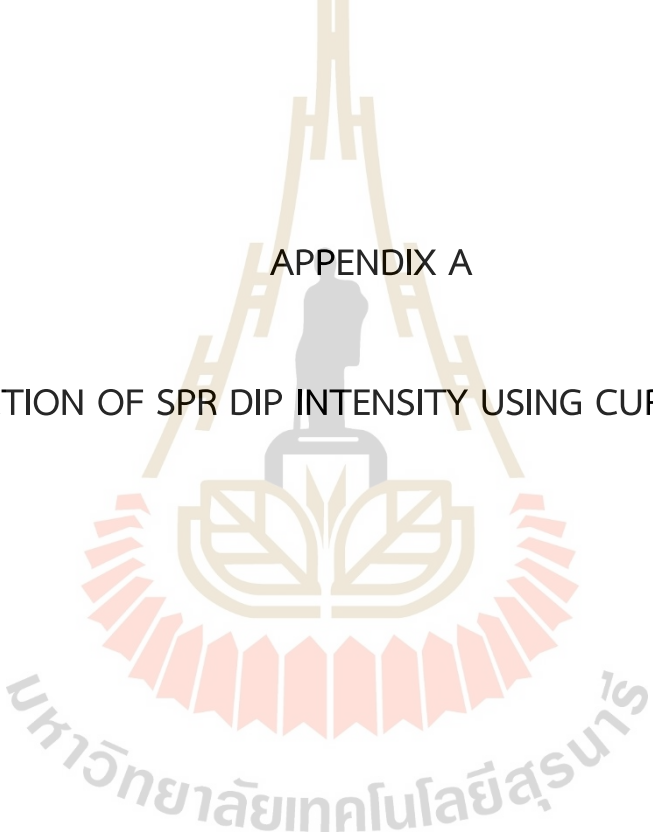
APPENDIX A

DETECTION OF SPR DIP INTENSITY USING CURVE FITTING
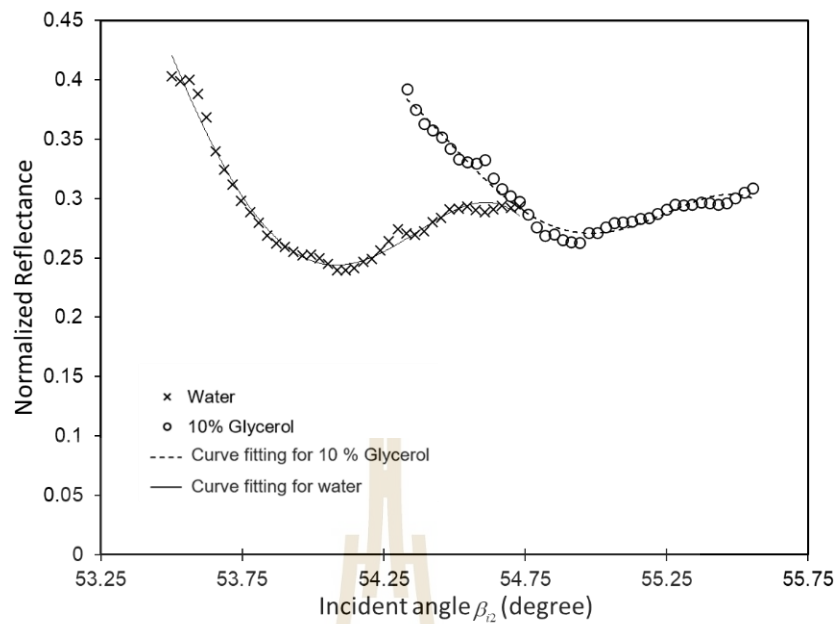
Figure A1 SPR reflectivity pattern of water and 10% glycerol averaged along the vertical direction of Fig. 4.5 and its corresponding curve fitting with the polynomial function order = 3 from 40 data points around the minimum dip intensity of the reflectivity patterns by using MATLAB.
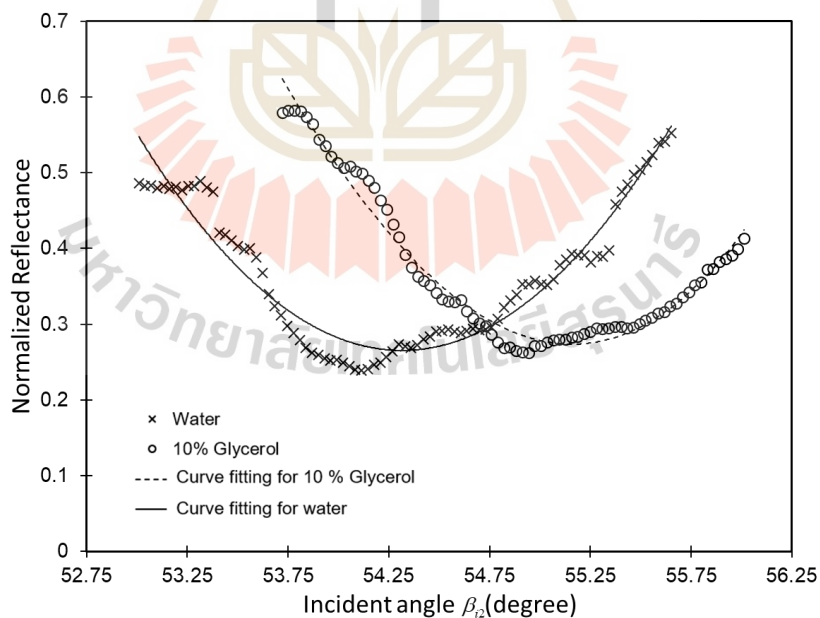
Figure A2 SPR reflectivity pattern of water and 10% glycerol averaged along the vertical direction of Fig. 4.5 and its corresponding curve fitting with the polynomial function order = 3 from 80 data points around the minimum dip intensity of the reflectivity patterns by using MATLAB.
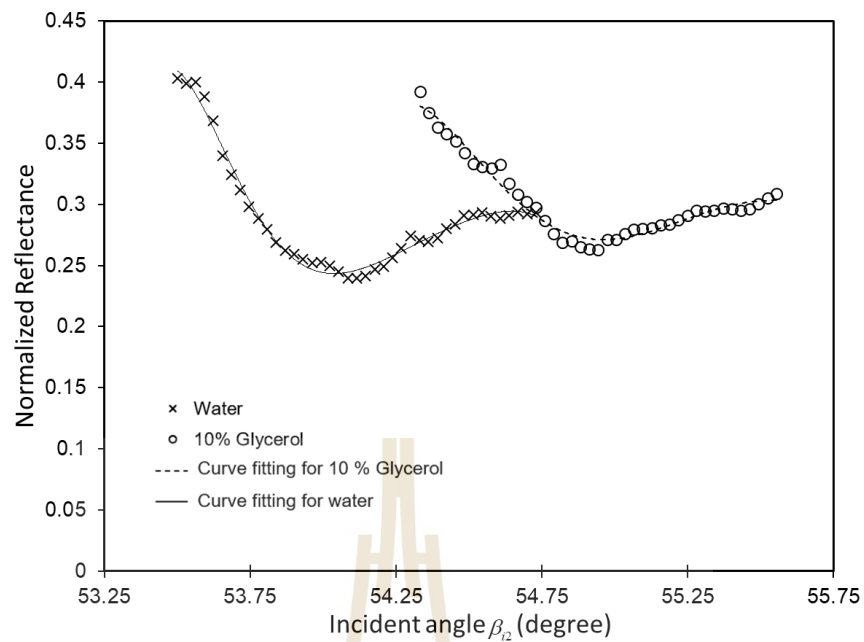
Figure A3 SPR reflectivity pattern of water and 10% glycerol averaged along the vertical direction of Fig. 4.5 and its corresponding curve fitting with the polynomial function order = 5 from 40 data points around the minimum dip intensity of the reflectivity patterns by using MATLAB.
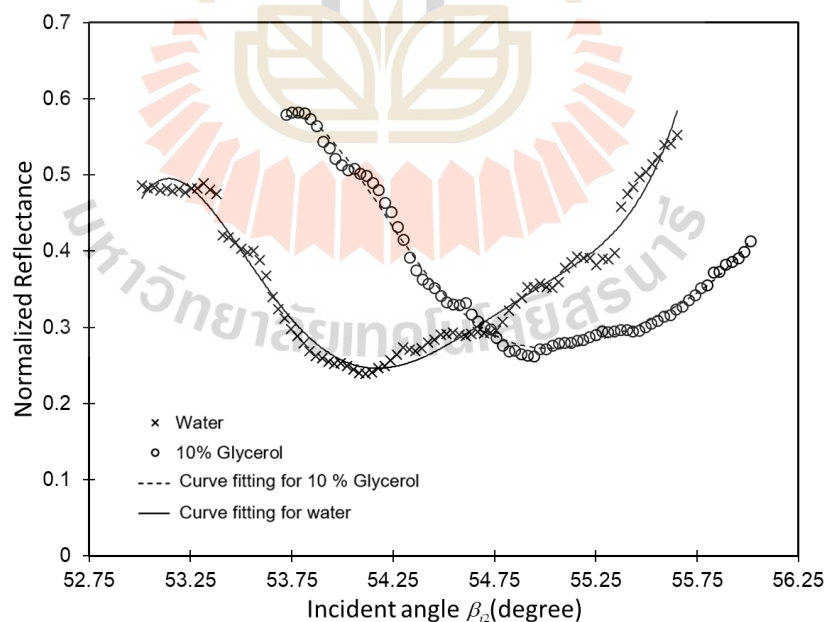
Figure A4 SPR reflectivity pattern of water and 10% glycerol averaged along the vertical direction of Fig. 4.5 and its corresponding curve fitting with the polynomial function order = 5 from 80 data points around the minimum dip intensity of the reflectivity patterns by using MATLAB.

In this Appendix, the detection of the SPR dip intensity discussed in Chapter 4 is compared with a polynomial curve fitting. The obtained SPR reflectivity signals were polynomially fitted by using polyfit(x,y,n) function of MATLAB program. The function employs the polynomial model

$$p(x)=p_1 x^n+p_2 x^{n-1}+...+p_n x+p_{n+1}. \tag{A.1}$$

The fitting gives the coefficients for a polynomial $p(x)$ of order n that is a best fit for the data in y.

Figure A1 and A3 show the SPR reflectivity pattern of water and 10% glycerol averaged along the vertical direction of Fig. 4.5 and its corresponding curve fitting with the polynomial function orders = 3 from 40 and 80 data points around the minimum dip intensity of the SPR reflectivity, respectively. Although higher accuracy of curve fitting can be obtained from a small number of data points, this Appendix fitted the SPR resonance angle from 40 and 80 data points around the minimum dip intensity. This is because fitting with fewer data points failed to detect the resonance angle. In comparison with Figs. A1 and A3, Figs. A2 and A4 show that the more data points that are fitted, the higher order of the polynomial fitting is required.

Tables A1 and A2 show the SPR angles and the RIs detected from 40 data points as a function of the fitting orders, while Tables A3 and A4 are the detection results from 80 data points. The four tables show that the 80 data points with the fitting order of 4 have an average error and SD detection results that are smaller than 0.1%. In the case of 40 data points, the best detection needs to be done with the third order of the fitting. In conclusion, the result of the curve fittings confirms the validity of the minimum dip detection in the experimental verifications.

Table A1 SPR angle detected by curve fittings with different orders of polynomial function from 40 data points around the minimum dip intensity calculated with MATLAB.

Glycerol concn (%)	Theoretical SPR angle	2nd order			3rd order			4th order			5th order		
		SPR angle	% error	SD	SPR angle	% error	SD	SPR angle	% error	SD	SPR angle	% error	SD
0	54.104	54.063	0.075	0.040069	54.115	0.020	0.025665	54.110	0.01	0.027084	54.116	0.022	0.027092
1	54.189	54.173	0.030	0.019799	54.212	0.043	0.011898	54.214	0.046	0.013275	54.214	0.046	0.013736
2	54.266	54.233	0.061	0.019328	54.290	0.043	0.029691	54.283	0.031	0.031948	54.287	0.039	0.031379
3	54.351	54.290	0.11	0.039127	54.33	0.036	0.031478	54.333	0.033	0.031633	54.341	0.019	0.024554
4	54.435	54.368	0.12	0.046198	54.424	0.020	0.029781	54.423	0.023	0.033069	54.423	0.021	0.032968
5	54.513	54.484	0.053	0.019799	54.518	0.009	0.007071	54.517	0.007	0.010801	54.523	0.017	0.008219
6	54.599	54.602	0.005	0.000471	54.622	0.043	0.014817	54.621	0.040	0.016997	54.621	0.040	0.016872
7	54.684	54.656	0.051	0.025456	54.693	0.02	0.026196	54.692	0.01	0.029033	54.694	0.018	0.028178
8	54.763	54.739	0.044	0.002828	54.767	0.008	0.017327	54.732	0.057	0.041963	54.769	0.01	0.018625
9	54.856	54.825	0.057	0.009428	54.866	0.02	0.030243	54.865	0.016	0.032782	54.869	0.024	0.029132
10	54.942	54.927	0.028	0.000943	54.929	0.023	0.004989	54.929	0.024	0.005715	54.929	0.024	0.006128

Table A2 RI detected by curve fittings with different orders of polynomial function from 40 data points around the minimum dip intensity calculated with MATLAB.

Glycerol concn (%)	Theoretical RI	2nd order			3rd order			4th order			5th order		
		RI	% error	SD	RI	% error	SD	RI	% error	SD	RI	% error	SD
0	1.3317	1.3311	0.05	0.000566	1.3319	0.01	0.000368	1.3318	0.008	0.000374	1.3319	0.01	0.000368
1	1.3329	1.3327	0.02	0.000283	1.3332	0.03	0.000189	1.3333	0.03	0.00017	1.3333	0.03	0.00017
2	1.3340	1.3335	0.04	0.000283	1.3343	0.02	0.000403	1.3343	0.02	0.00045	1.3343	0.02	0.000432
3	1.3352	1.3343	0.07	0.000566	1.3349	0.02	0.00045	1.3349	0.02	0.00045	1.3351	0.01	0.000309
4	1.3364	1.3355	0.070	0.00066	1.3363	0.01	0.000419	1.3362	0.01	0.000464	1.3362	0.01	0.000464
5	1.3375	1.3371	0.03	0.000283	1.3376	0.005	9.43E-05	1.3376	0.005	0.00017	1.3376	0.01	0.000125
6	1.3387	1.3387	0	0.00012	1.3390	0.02	0.000216	1.3390	0.02	0.000216	1.3390	0.02	0.000216
7	1.3399	1.3395	0.03	0.00033	1.3401	0.01	0.000368	1.3400	0.007	0.000408	1.3400	0.01	0.000411
8	1.3410	1.3406	0.03	4.71E-05	1.3411	0.005	0.000262	1.3406	0.03	0.000579	1.3411	0.005	0.000283
9	1.3423	1.3419	0.03	0.000141	1.3424	0.01	0.00045	1.3424	0.01	0.00045	1.3425	0.01	0.000374
10	1.3435	1.3433	0.01	0.00045	1.3433	0.01	4.71E-05	1.3433	0.01	8.16E-05	1.3433	0.01	8.16E-05

Table A3 SPR angle detected by curve fittings with different orders of polynomial function from 80 data points around the minimum dip intensity calculated with MATLAB.

Glycerol concn (%)	Theoretical SPR angle	2nd order			3rd order			4th order			5th order		
		SPR angle	% error	SD	SPR angle	% error	SD	SPR angle	% error	SD	SPR angle	% error	SD
0	54.104	54.109	0.009	0.010198	54.117	0.023	0.009031	54.114	0.019	0.006799	54.116	0.022	0.008287
1	54.189	54.204	0.028	0.015513	54.208	0.034	0.002867	54.205	0.030	0.004028	54.207	0.034	0.002867
2	54.266	54.256	0.018	0.03193	54.267	0.002	0.032934	54.270	0.008	0.034663	54.272	0.01	0.034567
3	54.351	54.324	0.050	0.016418	54.342	0.016	0.008994	54.342	0.017	0.009416	54.340	0.020	0.011324
4	54.435	54.436	0.001	0.04485	54.446	0.021	0.033039	54.442	0.013	0.043653	54.446	0.020	0.042898
5	54.513	54.497	0.029	0.021602	54.510	0.006	0.015107	54.506	0.01	0.017913	54.509	0.008	0.015923
6	54.599	54.594	0.009	0.004546	54.629	0.056	0.013597	54.619	0.037	0.019866	54.621	0.040	0.019328
7	54.684	54.691	0.01	0.006944	54.690	0.01	0.013597	54.693	0.02	0.008179	54.696	0.021	0.009286
8	54.763	54.770	0.013	0.008641	54.767	0.007	0.005793	54.764	0.002	0.004497	54.766	0.006	0.005312
9	54.856	54.831	0.045	0.015923	54.818	0.070	0.023228	54.821	0.063	0.017211	54.818	0.070	0.015195
10	54.942	54.929	0.023	0.013474	54.926	0.029	0.003559	54.928	0.026	0.0017	54.928	0.026	0.000943

Table A4 RI detected by curve fittings with different orders of polynomial function from 80 data points around the minimum dip intensity calculated with MATLAB.

Glycerol concn (%)	Theoretical RI	2nd order			3rd order			4th order			5th order		
		RI	% error	SD	RI	% error	SD	RI	% error	SD	RI	% error	SD
0	1.3317	1.3318	0.005	0.00017	1.3319	0.01	0.000125	1.3318	0.01	9.43E-05	1.3319	0.01	0.000125
1	1.3329	1.3331	0.02	0.000245	1.3332	0.02	4.71E-05	1.3331	0.02	4.71E-05	1.3332	0.02	4.71E-05
2	1.3340	1.3338	0.01	0.00045	1.3340	0	0.000455	1.3340	0.002	0.000499	1.3341	0.005	0.000464
3	1.3352	1.3348	0.03	0.000216	1.3351	0.01	0.000125	1.3351	0.02	0.000125	1.3350	0.01	0.00017
4	1.3364	1.3364	0	0.000638	1.3366	0.01	0.00045	1.3365	0.007	0.000638	1.3365	0.01	0.000618
5	1.3375	1.3373	0.02	0.000309	1.3374	0.005	0.000189	1.3374	0.007	0.000216	1.3374	0.007	0.000216
6	1.3387	1.3386	0.007	8.16E-05	1.3391	0.03	0.000205	1.3390	0.02	0.000283	1.3390	0.02	0.000283
7	1.3399	1.3400	0.007	8.16E-05	1.3400	0.007	0.000216	1.3400	0.007	9.43E-05	1.3401	0.01	0.000125
8	1.3410	1.3411	0.007	0.000141	1.3410	0	9.43E-05	1.3410	0	9.43E-05	1.3410	0	4.71E-05
9	1.3423	1.3420	0.02	0.000205	1.3418	0.04	0.00033	1.3418	0.03	0.000249	1.3418	0.03	0.000205
10	1.3435	1.3433	0.01	0.000205	1.3433	0.01	4.71E-05	1.3433	0.01	0	1.3433	0.01	0

Table A5 Comparison of % error and SD of SPR angle with different orders of polynomial function for 40 and 80 data points around the minimum dip intensity.

Average Values	2nd order		3rd order		4th order		5th order	
	40	80	40	80	40	80	40	80
% Error	0.058	0.022	0.025	0.025	0.027	0.022	0.028	0.025
SD	0.020313	0.017277	0.020832	0.014704	0.024936	0.015266	0.021535	0.015084

Table A6 Comparison of % error and SD of RI with different orders of polynomial function for 40 and 80 data points around the minimum dip intensity.

Average Values	2nd order		3rd order		4th order		5th order	
	40	80	40	80	40	80	40	80
% Error	0.033	0.013	0.015	0.015	0.016	0.013	0.015	0.015
SD	0.000339	0.000249	0.000297	0.000207	0.000347	0.000213	0.000294	0.000209
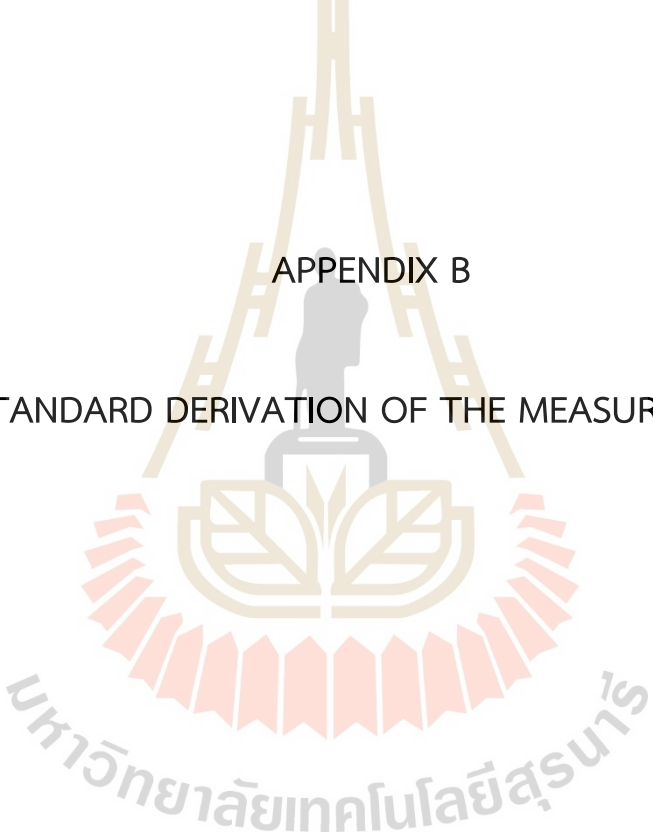
APPENDIX B

STANDARD DERIVATION OF THE MEASUREMENT

Table B1 Average and SD of detected pixels by using the proposed methodology.

Glycerol concentration (%)	Average positions of detected SPR dip (pixel)			Measured positions (pixel)	
	1st set of samples	2nd set of samples	3rd set of samples	Average	SD
0	1008	955	915	959	46.65119
1	1048	1039	1023	1037	12.66228
2	1117	1096	1104	1106	10.59874
3	1166	1168	1141	1158	15.04438
4	1268	1242	1223	1244	22.59056
5	1325	1312	1303	1313	11.06044
6	1407	1389	1376	1391	15.56706
7	1475	1452	1430	1452	22.50185
8	1557	1533	1524	1538	17.05872
9	1632	1611	1604	1616	14.57166
10	1693	1671	1644	1669	24.54248
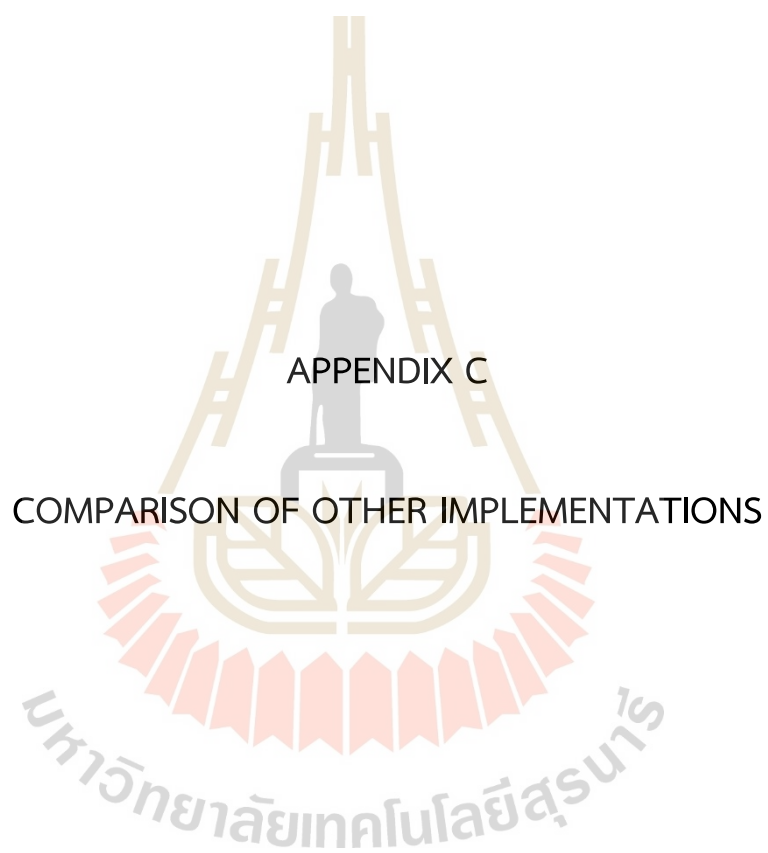
APPENDIX C

COMPARISON OF OTHER IMPLEMENTATIONS

As stated in the first chapter, introduction, Surface Plasmon Resonance, or SPR, is widely used in various fields. In this discussion, the prism coupling or Kretschmann configuration will be discussed. The fourth chapter of this thesis evaluates the performance of the suggested setup based on sensitivity and resolution which are 1.6375 × 10^{-5} RIU/pixel or 70.681°/RIU and 1.16 mdeg/pixel, respectively.

In the angular interrogation by using the chopper rotation (Patskovsky et al., 2013) as discussed in previous section. The laser source is He-Ne laser with wavelength of 632.8 nm. The sample to be measured are air, Ar and N$_2$ which have refractive index equal to 1, 1.000281 and 1.000298 were injected by the flow cell which can demonstrate the system for gas detection. Despite, the system being complex but is provides a sensitivity better than 10^{-6} RIU. The Δn from Ar to N$_2$ is around 1.7×10^{-5} RIU which is better than the proposed system because it can detect very small change of refractive index.

Furthermore, the Kretschmann configuration can be used in the wavelength interrogation (Bak et al., 2018) which is scanned the wavelength of the incident light and detected by CMOS camera with 2048 × 1088 pixel and pixel size 5.5μm × 5.5μm. It is achieved by using the wavelength-swept laser in the NIR region without mechanical movement and can detect a wide range of samples since the setup provides the beam with a 56 mm width. The wavelength-swept laser provides the single wavelength with a continuously sweeping wavelength by 50 nm from 770 nm to 820 nm (NIR range) with frequency 10 Hz. The samples to be detected are NaCl concentration 0-4% corresponding to refractive index 1.3330 to 1.3402 and SPR angle 54.196° to 54.706°. The refractive index varies linearly by an average interval of about 0.0018 as the concentration change which is higher than the proposed method that is 0.0012. The system can increase sensitivity up to 6501 nm/RIU and equal to

$$\text{Angular Sensitivity} = \frac{\Delta\theta}{\Delta n} = \frac{54.706° - 54.196°}{1.3402 - 1.3330} = 70.833°/RIU$$

which is slightly same as the proposed system. The resolution about 1.89 ×10^{-6} RIU with high dynamic range equal to 7.67×10^{-3} and multichannel by using flow-cell. In addition, it demonstrates interesting real-time measurements which can further use in

biomolecules and chemicals. Since the wavelength is longer provide the higher sensitivity than the proposed SPR system.
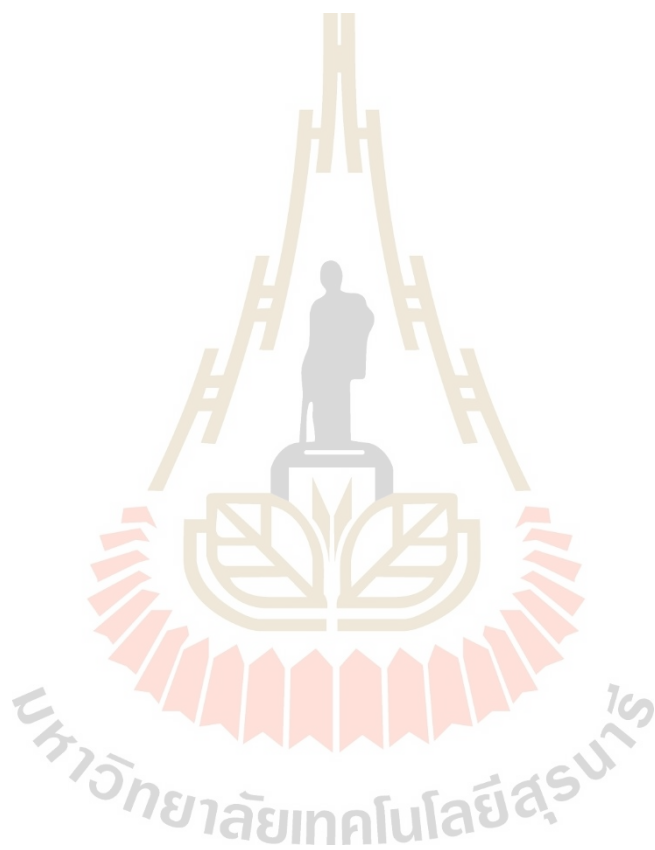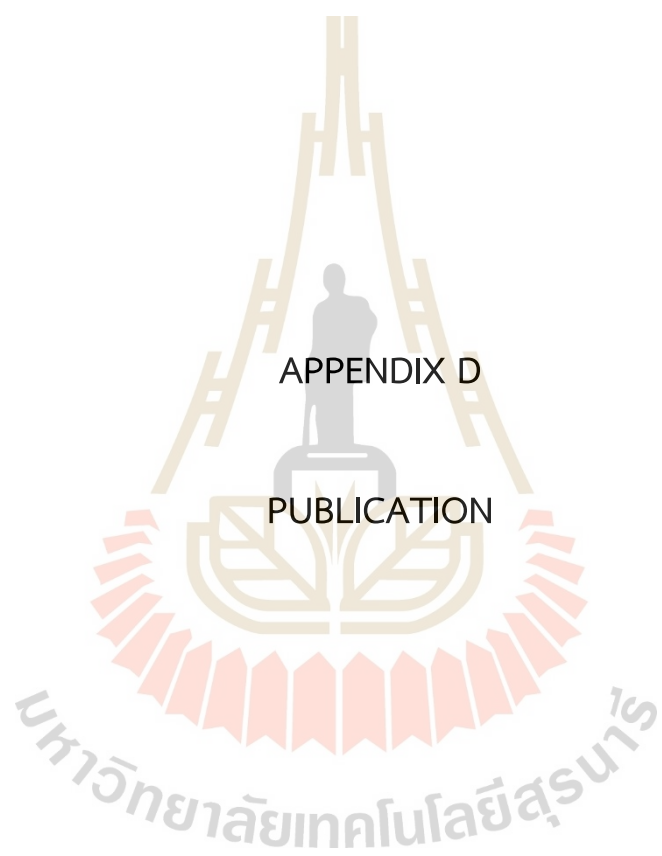
APPENDIX D

PUBLICATION

Publications that are related to this research work are included.

Netphrueksarat, W., and Widjaja, J. (2020, 4-6 March 2020). Development of Opto-electronic Biosenor based on Surface Plasmon Resonance Phenomenon using an Optical Relay Setup. Paper presented at the 2020 8th International Electrical Engineering Congress (iEECON).

Netphrueksarat, W., Widjaja, J., Hossea, J. H., and Meemon, P. (2022). Sensitivity enhancement of angular interrogation-based surface plasmon resonance sensor by using divergent beam illumination and digital interpolation. *Optik,* 270, 169936.

Development of Opto-electronic Biosensor based on Surface Plasmon Resonance Phenomenon using an Optical Relay Setup

Waramanee Netphrueksarat[*] and Joewono Widjaja[**]

[*]School of Electronic Engineering, [**]School of Physics
Suranaree University of Technology
111 University Avenue, Nakhon Ratchasima, Thailand
Email: [*]M6200459@g.sut.ac.th, [**]widjaja@sut.ac.th

Abstract — **Development of an opto-electronic biosensor based on surface plasmon resonance phenomenon is proposed by using an optical relay setup. The relay setup constructed using a 4-*f* optical architecture provides small divergent beam illumination inside a prism and resonates surface plasmons along an interface of dielectric and metal layers. Since size of a reflectivity output signal pattern is small, a compact sensor can be implemented by using a commercially-available small CMOS array image sensor.**

Keywords— *Surface plasmon resonance, opto-electronic sensor, refractive index sensor, biochemical sensor.*

I. Introduction

Surface plasmon resonance (SPR) sensor is the important optical biosensing technologies in many areas such as biochemistry [1], and medical sciences [2]. This is because it is a real-time [3], label-free [4], and also noninvasive nature [5]. In the SPR sensing, a small refractive index change of biochemical samples can be accurately detected. In this sense, SPR is widely used for detections of binding of the analyte to a ligand and antigen-antibody reaction [6]. To do this detection, parallel (p) polarized laser light is irradiated to an interface of a prism and a thin metallic film, where a biochemical sample being studied is placed [1]. When p-polarized light is incident on a certain angle greater than a critical angle on the interface of the prism and the metal, its energy is absorbed by free electrons in the metal's conduction band this resonates surface plasmons [7]. Consequently, totally reflected output light intensity becomes minimum. This incident angle is called the resonance angle [8].

In order to detect different samples, the irradiating laser light must be able to incident at various angles. Instead of mechanically rotating the laser orientation, the surface plasmons can also be resonated by irradiating divergent light beam onto the prism [9]. In the divergent beam configuration, the sample refractive index varies with respect to the spatial position of the sensing area. However, the drawback of this method is that the reflectivity output light intensity becomes very broad, causing difficulty in finding cheap and large-size array light sensors.

In this work, a new method for implementing divergent beam illumination is proposed by using an optical relay setup. The relay setup is constructed by using a 4-*f* optical architecture. It provides a small divergent illumination by focusing the illuminating beam inside the prism through a convex lens. When the focal plane of the lens is set closed to a sensing area, the resultant divergent beam size is small. As a result, commercially-available array image sensors can be used for the resonance detection. In addition, an angular sensitivity, which is defined as a ratio of the spatial change of the resonance angle to the change of the refractive index, is enhanced. Therefore, the relay setup solves major drawbacks of our previous SPR system [9], which is bulky and costly. In order to verify our proposed relay setup, the present work demonstrates experimentally the SPR sensing of air. Preliminary experimental results are in good agreement with the theory.

II. Surface Plasmon Resonance

The SPR is an optical phenomenon that occurs when photon energy of the incident light is absorbed by free electrons of the metal, resonating of the surface plasmons [10]. This can be achieved when the light incident on the prism produces an evanescent wave at the dielectric-metal medium [7]. This implies that the angle of incidence θ of the laser light must be greater than the critical angle or the total internal reflection occurs. When SPR occurs, the intensity of the totally reflected beam reduces drastically [8].

To achieve this resonance condition, the parallel wave vector of the evanescent wave

$$K_{evan} = \frac{2\pi}{\lambda} n_p \sin\theta \qquad (1)$$

must be equal to the wave vector of the surface plasmon

$$K_{sp} = \frac{2\pi}{\lambda} \sqrt{\frac{n_s^2 n_g^2}{n_s^2 + n_g^2}} , \qquad (2)$$

where n_p, n_s and n_g are refractive indices of the prism, the dielectric sample, and the metal, respectively [8].

Consequently, the matching wave vector K_{sp} and K_{evan} gives

$$\theta_{SPR} = \sin^{-1}\left(\frac{1}{n_p}\sqrt{\frac{n_s^2 n_g^2}{n_s^2 + n_g^2}}\right) \qquad (3)$$

with θ_{SPR} is the resonance angle for the dielectric sample. When this angle can be measured, the refractive index n_s of the sample is obtained by solving (3) [8].

III. Proposed SPR sensor

Fig. 1 shows a schematic diagram of the proposed opto-electronic SPR sensor using the optical relay setup. The sensing part consists of a prism, a gold-evaporated glass and a biochemical sample. The optical relay setup and a CMOS array image sensor act as the illumination and the detection parts, respectively. In the sensing part, the sample to be analyzed and a gold evaporated glass plate are placed in contact on top of an equilateral prism. In the relay setup, instead of Gaussian profile, Powell lens generates uniform beam distribution, while the 4-f optical setup focuses the beam in its rear focal point inside the prism. After passing the focal point, the beam is further diverged with its divergence angle determined by the beam size in the lens and its focal length. Furthermore, by aligning the focal point closed to the sensing area, the diverging beam size can be kept small, enhancing its sensitivity.
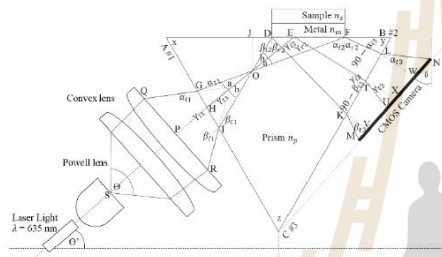
Fig. 1. Schematic diagram of the proposed opto-electronic SPR sensor using the optical relay setup.

The angle of incidences of the beams OD and OF, β_{i2} and α_{i2}, must cover resonance angles of the refractive index changes between n_p and n_s of the sample to be analyzed. To satisfy the resonance angle requirements, the divergence angle of the incident beam is set to

$$a + b = \alpha_{i2} - \beta_{i2}. \qquad (4)$$

As a consequence, the optical axis of the laser light source must be oriented with the angle

$$\theta' = \frac{z}{2} + \gamma_{r1} \qquad (5)$$

with respect to the horizontal axis. Here, γ_{r1} is given by

$$\gamma_{r1} = \sin^{-1}(n_p \sin(a - \alpha_{i2} + x)). \qquad (6)$$

When the convex lens with a focal length f is positioned at a distance PH from the prism side AC, the size of beam GI is given to

$$GI = 2\left[\frac{(BFL - PH)\sin\frac{\theta}{2}}{\sin(90 - (\sin^{-1}(n_p(x - \beta_{i2}))))}\right], \qquad (7)$$

where BFL is the back focal length of the convex lens. As a result, the size of the sensing and the detection areas are determined by the beams DF and MN, respectively. They are given by

$$DF = \frac{AG \sin(90 + \alpha_{i2} - x)}{\sin(90 - \alpha_{i2})}$$
$$- \frac{(AG - GI)\sin(90 - x + \beta_{i2})}{\sin(90 - \beta_{i2})}. \qquad (8)$$

The output beam is

$$MN = \frac{KL \cos \alpha_{t3} \sin\frac{(\beta_{t3} + \alpha_{t3})}{2}}{\cos\frac{(\beta_{t3} + \alpha_{t3})}{2}\sin\frac{(\beta_{t3} + \alpha_{t3})}{2}}$$
$$+ \frac{KV \cos\frac{(\beta_{t3} - \alpha_{t3})}{2}(\cos \alpha_{t3} - \cos \beta_{t3})}{\cos\frac{(\beta_{t3} + \alpha_{t3})}{2}\sin\frac{(\beta_{t3} + \alpha_{t3})}{2}}, \qquad (9)$$

where

$$\beta_{t3} = \sin^{-1}(n_p(\sin^{-1}(y - \beta_{i2}))) \qquad (10)$$

and

$$\alpha_{t3} = \sin^{-1}(n_p(\sin^{-1}(\alpha_{i2} - y))), \qquad (11)$$

respectively.

In the experimental verifications of the proposed SPR sensor, 15 mm N-SF11 equilateral prism was used as a medium to generate the evanescent wave. A gold-evaporated glass plate (Nano SPR, BA1000) placed on top of the prism was used as the sensing chip. The p-polarized beam was obtain by passing laser light with wavelength 635 nm through a combination of a polarizing beam splitter and a half wave plate. The optical axis of the illuminating light was set at θ' = 78.8°. Uniform laser beam profile was obtained after the light passed through Powell lens with a fan angle of 45°. The convex lens of focal length 25 mm placed of the distance PH = 10 mm focused the uniform beam at the point O, giving the divergent beam DF incident on the sensing chip. After the total internal reflection, the output beam MN had the length of about 3.3 mm, which could be detected by 1/2.5 inch CMOS camera. In this experiment the output beam was projected onto a screen and captured by a camera.
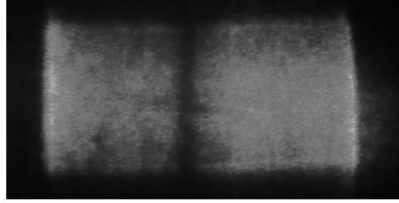
Fig. 2. Image of the SPR reflectance of air obtained by setting the half-wave plate to 0°.

Fig. 2 shows the image of the SPR reflectance of air by the p-polarized beam illumination which was obtained by setting the angle of the half wave plate to be 0°. The vertical dark line is the minimum dip reflectance caused by photon absorptions during the surface plasmon resonance at the gold-air interface.

Fig. 3 (a) and (b) are the reflectance intensities obtained by setting the half-wave plate to 22.5° and 45°, respectively. When the half-wave plate is set at 22.5°, the illuminating beam does not only have the p-component, but also the s-polarized component. Although the p-polarized wave energy is absorbed, the s-polarized component is totally reflected. This component reflection increases the total reflected intensity. Finally, in the last setting angle, the beam becomes the s-polarized wave. Therefore, it fails to resonate the surface plasmons.

(a)

(b)
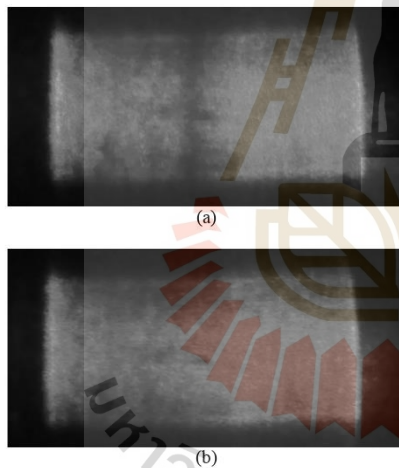
Fig. 3. Images of the SPR reflectance of air obtained by setting the half-wave plate to (a) 22.5° and (b) 45°, respectively.

Fig. 4 shows 1-D cross-sectional scans of the SPR reflectance shown in Figs. 2 and 3 as a function of the incident angle on the sensing chip. The solid, the dash-dotted and the dashed lines represent the intensities generated by the p-, the dual p-s- and the s-polarized lights, respectively. Comparison of the three reflected intensities show that the minimum dip intensity produced by the p-polarized light is clearly lower

than that of the p-s-polarized wave. In the case of the s-polarized wave, the minimum dip cannot be observed. These experimental results verify that the proposed optical relay setup can be used to resonate surface plasmons.
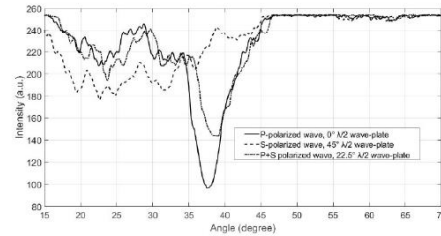
Fig. 4. 1-D cross sectional scans of the reflectance shown in Figs. 2 and 3.

Furthermore, Fig. 4 reveals that the experimental measurement of the resonance angle of air is equal to 37.62°. The difference between the experimental result and the theoretical value of 35.86° may be caused by misalignments of the relay setup and in particular the sensing chip. The resonance angle is shifted when the sensing chip is not uniformly placed in contact to the prism.

IV. CONCLUSIONS

We have proposed a new method for implementing the opto-electronic SPR sensor by using the optical relay setup. The relay setup is constructed by using the 4-*f* optical architecture. The proposed method has been experimentally verified by sensing the refractive index of air. The preliminary sensing result is in good agreement with the theory. The advantage of this set up is that the detected beam size is smaller than the previous work. Therefore, compact SPR biosensor can be implemented by using a cheap CMOS sensor.

REFERENCES

[1] A. V. Kabashin, S. Patskovsky, A N. Grigorenko, "Phase and amplitude sensitivities in surface plasmon resonance bio and chemical sensing," Optics Express, vol. 17, pp. 21191-21204, November 2009.
[2] F.Fathi, R. Jalili, M. Amjadi, M. Rashidi, "SPR signals enhancement by gold nanorods for cell surface marker detection," Bioimpact, vol 9, , pp. 67-70, October 2018.
[3] S. Bak, G. Kim, H. Jang, J. Kim, J. Lee, and C. Kim, "Real-time SPR imaging based on a large area beam from a wavelength-swept laser," Optics Lettler, vol. 43, pp. 5476-5479, November 2018.
[4] V. Kodoyianni, "Label-free analysis of biomolecular interactions using SPR imaging," BioTechniques, vol. 50 , pp. 32-40, January 2011.
[5] S. Firdous,S. Anwar, and R Rafya, "Development of surface plasmon resonance (SPR) biosensors for use in the diagnostics of malignant and infectious diseases," Laser Physics Letters, vol. 15, pp. 065602-065612, April 2018.

[6] M. Puiu and C. Bala, "SPR and SPR Imaging: Recent Trends in Developing Nanodevices for Detection and Real-Time Monitoring of Biomolecular Events," Sensor, vol. 16, pp. 870-885, June 2016.

[7] S. G. Ilchenko, R. A. Lymarenko and V. B. Taranenko, "Metal-Multilayer-Dielectric Structure for Enhancement of s- and p-Polarized Evanescent Waves" Nanoscale Research Letters, vol. 11, pp. 42-44, February 2016.

[8] Y. Tang, X. Zeng, and J. Liang, "Surface Plasmon Resonance: An Introduction to a Surface Spectroscopy Technique," NIH Public Access, vol. 87, pp. 742–746, July 2010.

[9] J. H. Hossea and J. Widjaja, "Design of surface plasmon resonance biosensors by using Powell lens," International Electrical Engineering Congress Pattaya Thailand, pp. 1-4, October 2017.

[10] Y. Zeng, L. Wang, S. Wu , J. He , J. Qu, X. Li, H. Ho, D. Gu, B. Gao and Y. Shao, "Wavelength-Scanning SPR Imaging Sensors Based on an Acousto-Optic Tunable Filter and a White Light Laser," Sensor, vol. 17, pp. 90-99, January 2017.

Sensitivity enhancement of angular interrogation-based surface plasmon resonance sensor by using divergent beam illumination and digital interpolation

Waramanee Netphrueksarat [a], Joewono Widjaja [b,*], Jordan H. Hossea [a], Panomsak Meemon [b]

[a] School of Electronic Engineering, Suranaree University of Technology, 111 University Avenue, Nakhon Ratchasima, Thailand
[b] School of Physics, Suranaree University of Technology, 111 University Avenue, Nakhon Ratchasima, Thailand

ABSTRACT

Sensitivity enhancement of an angular interrogation-based surface plasmon resonance sensor by using divergent beam illumination and digital interpolation is proposed. A small divergent beam of illumination generated inside a prism with a 4f optical setup provides a linear response of refractive index measurements, while a digital interpolation of surface plasmon resonance reflectance captured by using a moderate resolution image sensor enhances the angular resolution and the sensitivity without significantly increasing errors in the measurement. The proposed method is experimentally verified by varying glycerol concentrations from 0 % to 10 % w/w. The experimental results show that the sensitivity of about 10^{-7} RIU could be achieved without sophisticated interferometric instrumentation and computational complexity.

1. Introduction

Surface plasmon resonance (SPR) is an optical phenomenon that occurs when parallel (*p*) polarized laser light is incident on an interface of a dielectric medium and a metal layer at an angle greater than the critical angle of the two media [1]. In order to produce a resonant state of surface plasmons at the media interface, the incident photon must have the same wave vector and momentum as those of the plasmons. This resonance condition can be satisfied by adjusting the photon incident angle. At a particular angle known as the resonance angle, the plasmon resonance results in the absorption of the incident photon's energy by a sample placed on top of the metal layer. As a result, a dark band forms on a particular part of a reflected light pattern. Since wave vectors depend on refractive indices, a detection of the dark band using light sensors could be used for measuring the refractive index of the dielectric sample.

Useful applications of SPR sensor in a variety of fields, including medicine [2] and biochemistry [3] have been reported. Besides being able to detect changes in sample refractive index in real time [4,5], SPR sensor is label-free [6] and noninvasive [7]. SPR sensors can detect minute changes in the refractive index of low-volume samples with less preparation time than other chemical approaches [8]. SPR sensor is useful for healthcare monitoring [9], such as ovarian cancer diagnosis [10] and measurement of specification of morphine in urine samples [11]. Recently, successful detection of ligan and antigen-antibody reactions and CO_2 for indoors and outdoors were reported [12,13].

One of useful methods for implementing SPR sensors is the Kretschmann configuration, which consists of a prism, a gold thin layer as a sensor chip, and a dielectric sample to be analyzed. In the Kretschmann configuration, the incident light beam reaches the sensor chip's interface from inside the prism. When the plasmon resonance condition is met, photon energy from the incident beam is absorbed, resulting in a dip intensity in the reflected light at the resonance angle. Since the resonance angle depends on the refractive index of samples, different types of samples can be detected by varying the incident angle of photons. This SPR sensing is known as the angular interrogation method, because it analyzes samples based on the angular sensing response. The angular interrogation can be accomplished by rotating either a light laser source or the prism, which causes an increase in the sensor system's complexity and size [14–17]. Instead of the rotation systems, a vibrating mirror has also been used to change the angle of the illuminating laser beam [18]. The rotation and vibration scanning systems are bulky, and the scanning repeatability may cause backlash errors. To tackle this problem, a light emitting diode [19], a cylindrical lens [20] and a quantum cascade laser [21] and a laser diode [22] have been employed for implementing the SPR sensor. This is due to the fact that the diverging beam is made up of a bundle of light rays traveling at different angles. The beams, however, have a Gaussian electric field profile, which may degrade the SPR reflectance, resulting in a curvy dark band pattern rather than a well-defined SPR reflectivity dip.

A Powell lens, sometimes known as a laser line generator, generates a uniform line-shaped convergent beam from laser light [23]. Several methods for implementing SPR sensors using Powell lens SPR sensors have been proposed. An implementation of a multi-channel SPR has been proposed by translating a small divergent beam generated at the interface between the prism and the metal layer where an array of samples is placed. The beam translation is done by moving the Powell lens coupled to a laser source using a translation stage [24,25]. Therefore, this approach suffers from similar mechanical scanning problems. The second proposal employs Fourier transforming property of a thin lens to refract an incident parallel beam toward a back focal plane. When the lens is illuminated by a spatially shifted parallel beam, the output beam will be refracted with different angle of refractions. Therefore, the angular interrogation can be implemented by scanning the input divergent beam with a rotating slit and placing a metal layer on the back focal plane of the lens [26]. However, a rotating motor causes noise and vibration that affect measurement results. To solve this problem, a method for implementing the SPR system using a Powell lens without mechanical movement was reported [27]. This is simply achieved by directly illuminating the three-layer Kretschmann setup with a divergent beam generated from Powell lens. Besides being free from noise and vibration, a broad evanescent wave generation has an advantage over the previous methods in that different refractive indices of multiple samples can be simultaneously measured in a real time by using the simple setup. However, refraction of the beam occurred both inside and outside the prism broadens the output beam size incident on the light detector. This requires an expensive and large image sensor size.

In the present work, we propose a new method for enhancing the SPR sensitivity using a small divergent beam illumination and a digital interpolation technique detected by using a commercial image sensor. Unlike the previous method [27], the output beam from Powell lens is imaged inside the prism using a 4f optical setup, producing a small incident beam on the gold sensor chip. Besides preserving a broad divergence angle of the generated beam inside the prism, the 4f setup provides a linear response of refractive index measurements and increases the SPR sensitivity. In conjunction with interpolating digitally the SPR reflectivity signals captured using a moderate resolution image sensor, the proposed method could further enhance the SPR angular resolution and sensitivity without using sophisticated interferometric instrumentation or advanced computational algorithms [28–30]. A feasibility of the proposed method for implementing multi-channel SPR sensor is experimentally verified by measuring refractive indices of glycerol with concentrations 0–10 % (w/w).

2. Theory

2.1. Kretschmann prism configuration

In the three-layer Kretschmann configuration, the gold layer is sandwiched between the prism and the dielectric sample. When a wave vector of the illuminating light incident on the prism-gold interface matches to the plasmon wavevector [31].

$$K_{sp} = (2\pi/\lambda)\sqrt{n_s^2 n_g^2/(n_s^2 + n_g^2)}, \tag{1}$$

along the gold layer, the plasmons will resonate. Here λ, n_s and n_g are the wavelength of the incident light, the refractive indices of the dielectric sample and the gold layer, respectively. The matching condition can be satisfied by controlling the incident angle of the light at an angle that is larger than the critical angle. As a result, a refracted wave becomes an evanescent wave that propagates along the surface boundary and decays exponentially in amplitude along a path in the normal direction. From the above matching condition, the wave vector of the evanescent wave can be written as [32].

$$K_{evan} = (2\pi/\lambda)n_p \sin\alpha_i, \tag{2}$$

where n_p is the refractive index of the prism and α_i is the incident angle. Since the matching condition of the two wave vectors [1].

$$K_{sp} = K_{evan} \tag{3}$$

causes the resonance of the surface plasmon, this particular incident angle known as the resonance angle can be mathematically expressed as

$$\alpha_{SPR} = sin^{-1}\left[(1/n_p) \sqrt{n_s^2 n_g^2 / \left(n_s^2 + n_g^2 \right)} \; \right] \tag{4}$$

When the surface plasmon resonance occurs, the incident photon energy is absorbed by the electrons in the gold layer. As the result, the reflected light has a distinct dark band representing a minimum intensity. Detection of the dark band position results in the resonance angle α_{SPR}, which can then be used to calculate the refractive index of the sample according to Eq. (4). The resonance angle is useful not only for detecting samples, but also for designing SPR system components like types of prisms and metals that are appropriate for detecting certain sample.

2.2. Proposed SPR sensor using divergent beam illumination

Fig. 1 shows a schematic diagram of an optical setup for implementing the proposed Kretschmann-based SPR sensor by using a small divergent beam illumination. The plane of incidence of the illuminating beam is parallel to the xz plane. To reduce multiple light refractions, index matching liquid is fill between the gold-evaporated glass plate and the prism, while a sample to be tested is placed on top of the gold plate. Φ, χ and ψ are the angles of the apex and the vertexes A and B of the prism, respectively.

In the setup, Powell lens emits a uniform divergent line beam along the x axis with the angle of divergence θ. The beam is relayed into the prism by using the 4f optical system, consisting of two cylindrical lenses. The front focal plane of the first cylindrical lens is aligned with the focal point of the Powell lens, while that of the second lens is set at the desired point O inside the prism. However, due to the prism refraction, the focusing point shifts to the point O'. After the light refraction by the prism, the rays GF and ID shine the prism-gold interface at the angles α_{i2} and β_{i2}, respectively. These two angles correspond to the measurable refractive index variation between n_1 and n_2, with $n_1 < n_2$. Moreover, the angle γ_{i2} is the angle of incidence of the central ray HE. Note that the three angles must be greater than the critical angle of the prism. The reflected rays FL and DK are refracted into air and captured by a CMOS array image sensor. The captured SPR reflectivity pattern is then numerically analyzed in order to extract the resonance angle and the corresponding refractive index.

To satisfy the required resonance angles, α_{i2} and β_{i2}, the illuminating beam is set to form an angle at the focusing point inside the prism that can be obtained by considering triangles $\Delta DFO'$, which is

$$\phi + \varphi = \alpha_{i2} - \beta_{i2} \tag{5}$$

where $\phi + \varphi$ is the angle at the shifted focal point. As a consequence, the optical axis of the laser light source must be oriented at the angle

$$\theta' = (\Phi - \alpha_{i1} + \beta_{i1})/2 \tag{6}$$

with respect to the horizontal axis. In Eq. (6), α_{i1} and β_{i1} stand for the incident angles of the transmitted rays QG and RI on the surface #AC given by

$$\alpha_{i1} = sin^{-1}\left[n_p sin(\chi - \alpha_{i2}) \right] \tag{7}$$

and

$$\beta_{i1} = sin^{-1}\left[n_p sin(\chi - \beta_{i2}) \right] \tag{8}$$

respectively.

Furthermore, the optical setup must be aligned as follows. First, the distance PH must be smaller than the second lens' back focal
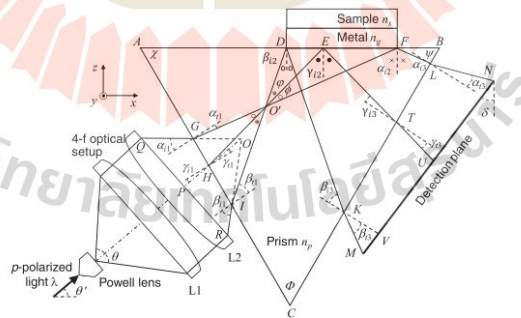
Fig. 1. Schematic diagram of the proposed divergent beam-based SPR sensor.

3

length (BFL). Secondly, the divergent beam width *DF*, which is the incident beam at the gold sensing part on the surface *#AB*, must be larger than the beam spot size at the focal point. From the two conditions, the input beam size *GI* can be derived by using the triangular ΔOGH and ΔOIH

$$GI = GH + HI = \{BFL - PH\sin[(\beta_{i1} - \alpha_{i1})/2]\}/(1/\cos\alpha_{i1} + 1/\cos\beta_{i1}) \tag{9}$$

When the incident position of the beam on the surface *#AC* is defined as *AG*, the size of the divergent beam *DF* at the sensing plate can be expressed as

$$DF = [(AG\cos\alpha_{i1})/(\cos\alpha_{i2})] - [(AG + GI)\cos\beta_{i1}/(\cos\beta_{i2})] \tag{10}$$

As a consequence, the sensing gold plate with the length *DF* has to be placed at the distance

$$AD = [(AG + GI)\cos\beta_{i1}]/\cos\beta_{i2} \tag{11}$$

from the vertex *A* on the surface *#AB* of the prism.

When the divergent beam is reflected from the boundary between the prism and the gold layer, it further diverges. At the surface *#BC*, the width of the divergent beam can be derived as

$$KL = \{[(AB - AD)\cos\beta_{i2}]/\cos(\psi - \beta_{i2})\}$$

$$-\{[(AB - AD - DF)\cos\alpha_{i2}]/\cos(\psi - \alpha_{i2})\} \tag{12}$$

where *AB* is the length of the prism hypotenuse. Due to the prism refraction, the refracted beams *KM* and *LN* are incident at different angles on a detection plane. In order to obtain uniform distribution of the incident angle of all refracted rays on the sensor plane, the plane must be inclined with respect to the vertical axis by the angle δ

$$\delta = 90 - \psi + [(\beta_{i3} + \alpha_{i3})/2]. \tag{13}$$

Here, α_{t3} and β_{t3} are equal to the angles α_{i1} and β_{i1}, respectively. The whole SPR reflectivity pattern can be captured by using an image sensor with a width *MN*. When the first and the last pixels of the image sensor are aligned with the rays *KM* and *LN*, respectively, the separation distance *KV* can be expressed as

$$KV = \{MN\cos[(\alpha_{i3} - \beta_{i3})/2] - KL\cos\alpha_{i3}\}$$

$$\times\{\cos[(\alpha_{i3} - \beta_{i3})/2]/\sin(\beta_{i3} - \alpha_{i3})\}/\cos[(\alpha_{i3} - \beta_{i3})/2] \tag{14}$$

with respect to the prism. On the other hand, the required sensor width may be determined by setting the separation distance *KV*. In this case, the sensor width is found equal to

$$MN = \{KV\sin(\beta_{i3} - \alpha_{i3})\cos[(\alpha_{i3} + \beta_{i3})/2]\}//\cos2[(\alpha_{i3} - \beta_{i3})/2]$$

$$+ (KL\cos\alpha_{i3})/\cos[(\alpha_{i3} - \beta_{i3})/2] \tag{15}$$

Eq. (14) sets the condition for the full utilization of the image sensor with the width *MN*, while Eq. (15) provides the condition for selecting the image sensor for a given separation distance *KV*. Since the width of the reflected beam *KL* is known, the pixel position of
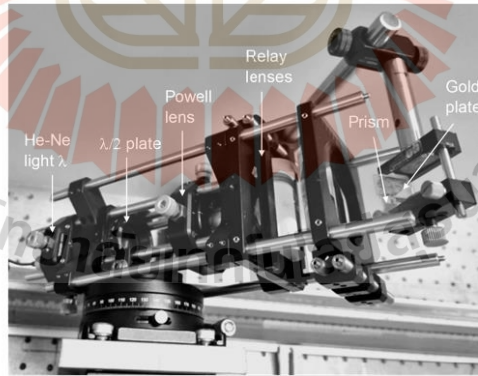
Fig. 2. Photograph of the optical setup for performing experimental verifications of the proposed divergent-beam-based SPR sensor.

the SPR dip intensity can be determined, yielding the measurements of the resonance angle and the corresponding refractive index.

3. Experimental verifications

In order verify feasibility of the proposed method, glycerol (n_{gly} = 1.4707) [33] with different concentrations were experimentally measured at room temperature of 25 °C by using the proposed SPR setup shown in Fig. 2. On the basis of Newton theoretical rule [34], the concentrations of glycerol were varied from 1 % to 10 % weight per weight (w/w) by diluting with water (n_w = 1.3317) [35]. Table 1 presents the calculated refractive index as a function of the glycerol concentration. It is apparent that the refractive index varies linearly by an average interval of about 0.0012 with respect to the concentration change. The last column of Table 1 gives the corresponding resonance angle calculated by using Eq. (4). To evaluate validity and reliability of the proposed SPR sensor, the refractive index measurements were compared with an Abbe refractometer (Atago, 1220 NAR-2T), which has a measurement range of 1.3000–1.7000. The experimental refractive index measurement of each concentration was repeated ten times.

The plasmon resonance was generated by sandwiching the gold-evaporated glass plate (Nano SPR, BA1000) with the refractive index n_g = 0.1728+j3.4218 [36] between the sample and a 15 mm N-SF11 equilateral prism with n_p = 1.785, Edmunds, #45-950. The index matching liquid (Series A; Cargille-Sacher Laboratories, Inc) was fill in the gap between the prism and the gold plate. The p-polarized beam was obtained by passing a laser light with a 635 nm wavelength (Thorlabs, #CPS635) via a half wave plate (Thorlabs, #WPH10E-633). The illuminating light's optical axis was fixed at the angle θ' = 59°. After passing through Powell lens with a 45° fan angle (Thorlabs, #PL0145), the 4f optical relay setup with 25 mm focal length focused the uniform divergent beam to the point O. The distances AG and PH were set equal to 5.5 mm and 15 mm, respectively. However, due to the prism refraction, the focusing point shifted to the point O' and the divergent beam incident on the sensing area had the angles varied from 33° to 58° This range of incident angles gave beam width DF of approximately 1.5 mm at the gold plate.

To minimize measurement errors, each glycerol sample was simultaneously measured with water as a reference for calibration. Fig. 3(a) shows two droplets of water and 10 % glycerol solution placed side-by-side in the y-axis on top the gold plate by using a 10-microliter pipette (Brandtech, Transferpette S Pipette). The alignment of the samples along the y-axis demonstrates that the proposed setup can be utilized for multi-channel measurements. The corresponding SPR reflectivity pattern of the samples is depicted in Fig. 3 (b). The x- and y-axes on the pattern captured by the sensor correspond to the horizontal and the vertical directions of light distribution on the gold plate. Since the beam incident on the gold plate diverges in the x direction, the angle of incidence of the light beam on the gold plate is mapped to position along the x-axis of the pattern. The vertical size of the pattern was about 200 pixels. It is apparent that there are two dark bands appeared in different positions along the x and the y directions. The top dark band corresponds to the SPR dip intensity of water, while the bottom one is caused by 10 % glycerol solution. The bright intensity pattern between the dark bands corresponds to the light reflected from the area between the two sample droplets in Fig. 3(a). Their horizontal positions reveal that the resonance angle of water is smaller than that of the 10 % glycerol solution. They are in agreement with Table 1.

Fig. 4 plots cross-sectional SPR reflectivity of water and glycerol solution shown in Fig. 3(b). Each scanned reflectivity represents the average intensity of fifty pixels along the vertical direction. The dip intensities of the SPR reflectivity of water and glycerol appear around the angles of 54° and 55°, respectively. The reflectivity curve of glycerol is slightly broader than that of water, because its refractive index is higher. The experiment result demonstrated the feasibility of the proposed method for single shot measurement of multi-channel refractive index.

In order to measure the refractive index of each glycerol concentration, the CMOS sensor (Basler, daA2500–14 μm) with 2592 pixel × 1944 pixel in an area of 5.7 mm × 4.3 mm was inclined with respect to the vertical axis at the angle δ of about 39°. The distance KV was set to 56 mm with the distance MV was 7 mm. As a result, the whole length of the sensor could detect the light beam incident at the angle of 53° to 56° on the gold plate, yielding the angular resolution of 1.1574 mdeg/pixel. The resolution of the proposed method is improved by about two and half times compared with 0.00289° of the previous divergent beam-based SPR sensor [27].

Fig. 5 plots the average position of the experimentally detected SPR dips as a function of the sample refractive index presented in Table 1. The circle represents the average dip position, while the solid line is the linear regression line $y = 60{,}996x - 80{,}269$ that best fits the detected dip positions. The calculated coefficient of determination R^2 gives 0.99896. This indicates that the detected dip intensity position has a positive linear relationship with the increase in the sample refractive index. According to the regression line, the

Table 1
Calculated refractive index and resonance angle as a function of the glycerol concentration.

Glycerol Concn. (%)	Refractive Index n_s	α_{SPR} (°)
0	1.3317	54.104
1	1.3329	54.189
2	1.3340	54.266
3	1.3352	54.351
4	1.3364	54.435
5	1.3375	54.513
6	1.3387	54.599
7	1.3399	54.684
8	1.3410	54.763
9	1.3423	54.856
10	1.3435	54.942

Fig. 3. (a) Droplets of water and 10 % glycerol on top of the gold plate and (b) the corresponding SPR reflectivity pattern.
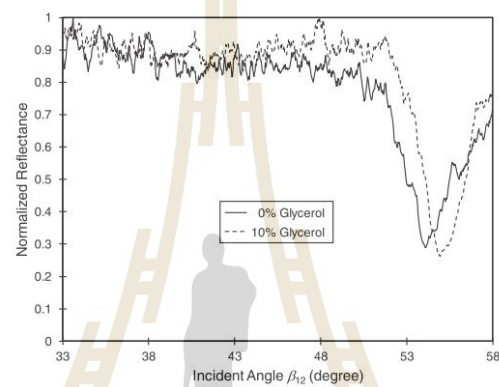
Fig. 4(. a) SPR reflectivity pattern of water and 10 % glycerol averaged along the vertical direction.
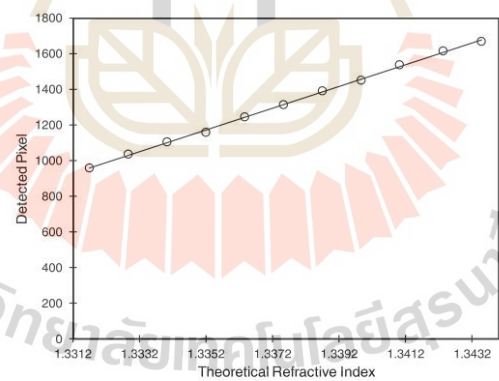
Fig. 5. Average positions of the experimentally detected dip intensity as a function of the refractive index.

proposed sensor has the sensitivity of 1.6395×10^{-5} RIU/pixel equivalent to 70.595°/RIU, which is higher than the previous method [27]. According to Homola [37], the theoretical sensitivity of the proposed setup is about 70.089°/RIU. After averaging the detected dip positions, the resultant average value was used to obtain the resonance angle. Finally, the refractive index of the sample was

calculated by solving Eq. (4). Besides the sensitivity, which is the most significant performance parameter of the SPR sensor, the full width at half-maximum (FWHM) of the SPR reflectance curve and the efficiency of the energy transfer of the electromagnetic wave to the surface plasmon wave [38,39] were calculated to give better insight into the performance of the proposed sensor setup. The FWHM of water and of the 10 % glycerol are 1.97° and 2.14°, respectively. Water has a narrower FWHM than 10 % glycerol solution because, for the lower refractive index sample, the transfer of photon energy occurs in the narrower range of the angle of incidence. The SPR reflectivity curve is consequently sharpened. This is in agreement with the theory, which states that the FWHM is inversely proportional to the prism RI and the cosine of the sample resonance angle [39]. Finally, the transfer efficiency of the photon energy is found to be greater than 70 % both for water and glycerol solution.

Table 2 presents the mean absolute percentage errors (MAPEs) in measurements of the sample refractive indices and the corresponding resonance angles using the proposed method and the refractometer. In the table, RI stands for the refractive index, while the resonance angles were calculated by using the experimentally detected position of the dip intensities. A comparison of the mean absolute errors in measuring the refractive index of different glycerol concentrations via the proposed method and the refractometer shows that they tend to have small values of less than 0.1 %. It is worth pointing out that the overall errors of the proposed method never exceed those of the refractometer. Therefore, the experimental results verify the reliability and the validity of the proposed divergent beam generation inside the prism for implementing SPR sensors.

The experimental results presented in Table 2 show that the proposed method has small errors in the measurements of the glycerol refractive indices. This can be understood as follows: Although the proposed method has the same physical mechanism of resonance sensing as the conventional 3-layer configuration, the main difference between them is that the proposed method employs the uniform line-shaped divergent laser beam illumination generated by the Powell lens. The beam provides an infinite bundle of fan-shaped light rays with a uniform field distribution that impinges simultaneously on the sensing area at different angles. When the sample refractive index varies spatially along the sensing area within the range of the designed resonance angles α_{i2} and β_{i2}, the bundle of light rays provides a simultaneously infinite number of detectable resonance angles. Since each reflected light ray will be further diverged during the propagation through free space, the minimum dip positions will be separated from each other at the image sensor plane. Furthermore, the reflectance linearity obtained using the proposed method plays a crucial role in the detection accuracy of the dip minimum intensity. This is because the degradation of the SPR reflectance caused by the Gaussian beam issue is eliminated. Therefore, in conjunction with the conventional resonance optimization methods [37–43], the proposed method can facilitate further improvement of the performance of the SPR sensors.

Due to the positive linear relationship between the detected dip intensity position and the sample refractive index, the detectable dips can be improved by enhancing the angular resolution and the sensitivity of the SPR sensors. This can be implemented by using a linear interpolation technique. In the present work, the resultant 1-D scanned SPR signals were digitally interpolated by factors of ten, twenty and thirty using the interp1 function in Matlab 2018b. Since the interpolation increases the sample rate of the input signal, the total number of pixels of the interpolated SPR reflectivity became 25,920, 51,840 and 77,760, respectively. As a consequence, the resultant angular resolutions improved to 0.11574, 0.057870 and 0.038580 mdeg/pixel, respectively. Finally, the pixel position of the interpolated dip SPR intensity was detected in order to determine the resonance angle that gave the measured refractive index value. Fig. 6 shows plots of the average positions of the detected dip intensity obtained without and with the interpolations as a function of the theoretical refractive index. The circle symbol corresponds to the detected pixels obtained without interpolation as shown in Fig. 5. The square, the diamond and the triangle symbols denote the detected pixels using the interpolations by the factors of ten, twenty and thirty, respectively. It is understood that the slope of the linear regression line has becomes higher with increasing the interpolation factor. The enhancement of the angular resolution and the sensitivity together with the mean absolute percentage error in the refractive index measurement are summarized in Table 3. It is important to note that first, the interpolation with the factor of twenty-fold improves the sensitivity to become about 10^{-7} RIU/pixel with the angular resolution of 0.05787 mdeg/pixel. Secondly, the errors are always smaller than 1 %, regardless the interpolation factor. Finally, the enhancement of the angular resolution, the sensitivity, and the measurement accuracy can be achieved by using a moderate image sensor resolution without sophisticated interferometric instrumentation or computational complexity [28–30].

4. Conclusions

The new method for enhancing the SPR sensitivity using the small divergent beam illumination and the digital interpolation technique has been proposed and experimentally verified. The small divergent beam of illumination generated inside the prism using the 4f optical setup provides a linear response of the refractive index measurements, while the digital interpolation of the SPR reflectivity signals captured by using the moderate resolution image sensor causes the angular resolution and the sensitivity enhancements without significantly increasing the error in the measurements. The proposed method was experimentally verified by performing single shot refractive index measurements of two-channels of glycerol concentration varying from 0 % to 10 % w/w. The experimental results show that the proposed method could provide the sensitivity of about 10^{-7} RIU without sophisticated interferometric instrumentation and iterative computational algorithms.

Declaration of Competing Interest

The authors declare that they have no known competing financial interests or personal relationships that could have appeared to influence the work reported in this paper.

Table 2
Mean absolute percentage errors in measurements of the resonance angle and the refractive index of the ten samples using the proposed method and the refractometer.

| Sample Concn. (%)	Theory		Refractometer		Proposed Method			
	RI	α_{SPR} (°)	RI	MAPE (%)	α_{SPR} (°)	MAPE (%)	RI	MAPE (%)
0	1.3317	54.104	1.3318	0.008	54.110	0.01	1.3318	0.008
1	1.3329	54.189	1.3331	0.02	54.201	0.022	1.3331	0.02
2	1.3340	54.266	1.3342	0.01	54.280	0.026	1.3342	0.01
3	1.3352	54.351	1.3354	0.01	54.340	0.020	1.3351	0.007
4	1.3364	54.435	1.3363	0.007	54.440	0.007	1.3364	0.00
5	1.3375	54.513	1.3380	0.04	54.519	0.01	1.3376	0.007
6	1.3387	54.599	1.3390	0.02	54.610	0.020	1.3389	0.01
7	1.3399	54.684	1.3403	0.03	54.681	0.005	1.3399	0.00
8	1.3410	54.763	1.3413	0.02	54.780	0.031	1.3412	0.01
9	1.3423	54.856	1.3430	0.05	54.871	0.027	1.3425	0.01
10	1.3435	54.942	1.3442	0.05	54.931	0.020	1.3434	0.007
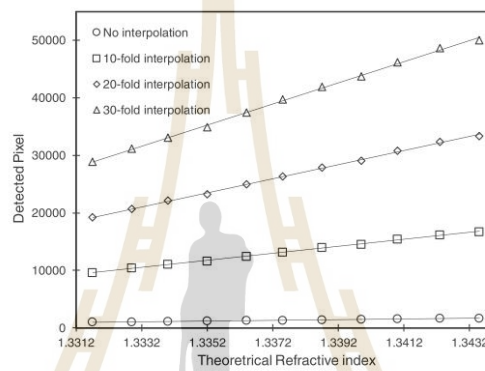
Fig. 6. Average positions of the experimentally detected dip intensity as a function of the refractive index with and without interpolations.

Table 3
Enhanced angular resolution and sensitivity by using the linear interpolation technique and the resultant mean absolute percentage errors in the measurements.

Interpolation Factor	R-squared	Angular Resolution (mdeg/pixel)	Sensitivity (RIU/pixel)	MAPE (%)
0	0.99877	1.1574	1.6395E-05	0.008
10	0.99872	0.11574	1.6375E-06	0.009
20	0.99876	0.057870	8.1768E-07	0.01
30	0.99864	0.003858	5.4520E-07	0.01

Data Availability

The data that has been used is confidential.

References

[1] R.B.M. Schasfoort (Ed.), Handbook of Surface Plasmon Resonance, The Royal Society of Chemistry, Croydon, 2017.
[2] F. Fathi, R. Jalili, M. Amjadi, M.R. Rashidi, SPR signals enhancement by gold nanorods for cell surface marker detection, BioImpacts 9 (2) (2019) 71–78.

8

[3] A.V. Kabashin, S. Patskovsky, A.N. Grigorenko, Phase and amplitude sensitivities in surface plasmon resonance bio and chemical sensing, Opt. Exp. 17 (2009) 21191–21204.
[4] S. Bak, G.H. Kim, H. Jang, J. Kim, J. Lee, C.S. Kim, Real-time SPR imaging based on a large area beam from a wavelength-swept laser, Opt. Lett. 43 (21) (2018) 5476–5479.
[5] J. Wang, R. Smith, Highly sensitive multipoint real time kinetic detection of Surface plasmon bioana- lytes with custom CMOS camera, Biosens. Bioelectron. 58 (2014) 157–164.
[6] V. Kodoyianni, Label-free analysis of biomolecular interactions using SPR imaging, BioTechniques 50 (1) (2011) 32–40.
[7] S. Firdous, S. Anwar, R. Rafya, Development of surface plasmon resonance (SPR) biosensors for use in the diagnostics of malignant and infectious diseases, Laser Phys. Lett. 15 (6) (2018) 65602–65607.
[8] Q. Liu, H. Yuan, Y. Liu, J. Wang, Z. Jing, W. Peng, Real-time biodetection using a smartphone-based dual-color surface plasmon resonance sensor, J. Biomed. Opt. 23 (4) (2018) 1–6.
[9] M. Puiu, C. Bala, SPR and SPR Imaging: recent trends in developing nanodevices for detection and real-time monitoring of biomolecular events, Sensors 16 (6) (2016) 870–884.
[10] B. Szymanska, Z. Lukaszewski, B. Zelazowska-Rutkowska, K. Hermanowicz-Szamatowicz, E. Gorodkiewicz, An SPRi biosensor for determination of the ovarian cancer marker HE4 in human plasma, Sensors 21 (10) (2021) 3567–3575.
[11] H. Ke, X. Du, L. Wang, Detection of morphine in urine based on a surface plasmon resonance imaging immunoassay, Anal. Methods 12 (2020) 3038–3044.
[12] N. Mudgal, A. Saharia, Modeling of highly sensitive surface plasmon resonance (SPR) sensor for urine glucose detection, Opt. Quantum Electron. 52 (2020) 1–14.
[13] F. Pérez-Ocón, A.M. Pozo, J. Cortina, O. Rabaza, Surface plasmon resonance sensor of CO_2 for indoors and outdoors, Appl. Sci. 11 (2021) 6869–6877.
[14] G. Lan, S. Li, Y. Ma, Sensitivity and figure-of merit enhancements of liquid-prism SPR sensor in the angular interrogation, Opt. Commun. 352 (2015) 49–54.
[15] J.A. Ruemmele, M.S. Golden, Quantitative surface plasmon resonance imaging: A simple approach to automated angle scanning, Anal. Chem. 80 (12) (2008) 4752–4756.
[16] O. Pluchery, R. Vayron, K.M. Van, Laboratory experiments for exploring the surface plasmon resonance, Eur. J. Phys. 32 (2) (2011) 585–599.
[17] I. Lundstrom, From a laboratory exercise for students to a pioneering biosensing technology, Plasmonics 9 (4) (2014) 741–751.
[18] A.T.M. Lenferink, R.P.H. Kooyman, J. Greve, An improved optical method for surface plasmon resonance experiments, Sens. Actuators B Chem. 3 (4) (1991) 261–265.
[19] T.M. Chinowsky, J.G. Quinn, D.U. Bartholomew, R. Kaiser, J.L. Elkind, Performance of the Spreeta 2000 integrated surface plasmon resonance affinity sensor, Sens. Actuators B Chem. 91 (1–3) (2003) 266–274.
[20] B.L. Chan, S. Jutamulia, Micro-prism test chip, US Patent Application Number 14/120,049, 2014.
[21] S. Herminjard, L. Sirigu, Surface plasmon resonance sensor showing enhanced sensitivity for CO_2 detection in the mid-infrared range, Opt. Exp. 17 (1) (2009) 293–303.
[22] S. Isaacs, I. Abdulhalim, Long range surface plasmon resonance with ultra-high penetration depth for self-referenced sensing and ultra-low detection limit using diverging beam approach, Appl. Phys. Lett. 106 (19) (2015), 193701.
[23] I. Powell, Linear Diverging Lens, US Patent US4826299 (A) 2, 1989.
[24] R. Chen, M. Wang, S. Wang, H. Liang, X. Hu, X. Sun, J. Zhu, L. Ma, M. Jiang, J. Hu, J. Li, A low-cost surface plasmon resonance biosensor using a laser line generator, Opt. Commun. 349 (2015) 83–88.
[25] J. Hu, B. Cao, S. Wang, J. Li, W. Wei, Y. Zhao, X. Hu, J. Zhu, M. Jiang, X. Sun, R. Chen, L. Ma, Design and fabrication of an angle-scanning based platform for the construction of surface plasmon resonance biosensor, Opt. Lasers Eng. 78 (2016) 1–7.
[26] S. Patskovsky, M. Meunier, Integrated Si-based nanoplasmonic sensor with phase-sensitive angular interrogation, Ann. Phys. 525 (6) (2013) 431–436.
[27] J. Widjaja, J. Hossen, Experimental validations of divergent beam illumination and detection conditions in a surface plasmon resonance sensor using a Powell lens, Lasers Eng. 48 (1–3) (2021) 17–32.
[28] L. Guoqiang, G. Yachen, Surface plasmon resonance sensor with high sensitivity and wide dynamic range, IEEE Sens. J. 18 (13) (2018) 5329–5333.
[29] A. Karabchevsky, S. Karabchevsky, I. Abdulhalim, Fast surface plasmon resonance imaging sensor using Radon transform, Sens. Actuators B Chem. 155 (1) (2011) 361–365.
[30] K. Thadson, S. Visitsattapongse, S. Pechprasarn, Deep learning-based single-shot phase retrieval algorithm for surface plasmon resonance microscope based refractive index sensing application, Sci. Rep. 11 (2021) 16289.
[31] S.A. Maier, Plasmonics: Fundamentals and Applications, Springer, New York, 2007.
[32] Y. Tang, X. Zeng, J. Liang, Surface plasmon resonance: an introduction to a surface spectroscopy technique, J. Chem. Educ. 87 (2010) 742–746.
[33] J. Rheims, J. Köser, T. Wriedt, Refractive-index measurements in the near-IR using an Abbe refractometer, Meas. Sci. Technol. 8 (6) (1997) 601–605.
[34] A. Gayathri, T. Venugopal, R. Padmanaban, A comparative study of experimental and theoretical refractive index of binary liquid mixtures using mathematical methods, IOP Conf. Ser.: Mater. Sci. Eng. 390 (2018) 1–4.
[35] G.M. Hale, M.R. Querry, Optical constants of water in the 200-nm to 200-μm wavelength region, Appl. Opt. 12 (1973) 555–563.
[36] M. Yamamoto, Surface plasmon resonance (SPR) theory: tutorial, Rev. Polarogr. 48 (3) (2002) 209–237.
[37] J. Homola, I. Koudela, S.S. Yee, Surface plasmon resonance sensors based on diffraction gratings and prism couples: sensitivity comparison, Sens. Actuators B Chem. 54 (1–2) (1999) 16–24.
[38] S. Patskovsky, A.V. Kabashin, M. Meunier, J.H.T. Luong, Properties and sensing characteristics of surface plasmon resonance in infrared light, J. Opt. Soc. Am. A 20 (8) (2003) 1644–1650.
[39] T.T. Nguyen, N.V. Sau, Q.M. Ngo, G. Eppe, N.Q. Tran, N.T.P. Anh, Enhanced sensitivity and detection of near-infrared refractive index sensor with plasmonic multilayers, Sensors 21 (7056) (2021) 1–15.
[40] G. Gupta, J. Kondoh, Tuning and sensitivity enhancement of surface plasmon resonance sensor, Sens. Actuators B Chem. 122 (2) (2007) 381–388.
[41] M.K. Singh, S. Pal, Y.K. Prajapati, Design and analysis of an SPR sensor based on Antimonene and Platinum for the detection of formalin, IEEE Trans. NanoBiosci. (2022).
[42] R. Kumar, S. Pal, Y.K. Prajapati, S. Kumar, J.P. Saini, Sensitivity improvement of a MXene-immobilized SPR sensor with Ga-Doped-ZnO for biomolecules detection, IEEE Sens. J. 22 (7) (2022) 6536–6543.
[43] M.K. Singh, S. Pal, A. Verma, R. Das, Y.K. Prajapati, A nanolayered structure for sensitive detection of hemoglobin concentration using surface plasmon resonance, Appl. Phys. A Mater. Sci. Process 127 (11) (2021) 1–10.

BIOGRAPHY

Mrs. Waramanee Netphrueksarat was born on October 30, 1996 in Nakhon Ratchasima, Thailand. She earned her Bachelor's Degree in Electronic Engineering from Suranaree University of Technology (SUT) in 2018. She then continued her Master's degree in Electronic Engineering at School of Electronic Engineering, Institute of Engineering at Suranaree University of Technology. Her fields of interest include the field of laser and optical sensors. During her Master's degree study, she presented an international paper entitled of "Development of Opto-electronic Biosensor based on Surface Plasmon Resonance Phenomenon using an Optical Relay Setup" in the 2020 International Electrical Engineering Congress, Chiang Mai, Thailand, and published one international journal entitled of "Sensitivity enhancement of surface plasmon resonance angular-interrogation sensor by using divergent beam illumination and digital interpolation" in Optik International Journal for Light and Electron Optics 2022.